Causality-Enriched Epigenetic Age Uncouples Damage and Adaptation

Kejun Ying[1,2], Hanna Liu[1,3,4], Andrei E. Tarkhov[1], Marie C. Sadler[5,6,7], Ake T. Lu[8,9], Mahdi Moqri[1,10], Steve Horvath[8,9], Zoltán Kutalik[5,6,7], Xia Shen[11,12,13,14], Vadim N. Gladyshev[1,]

[1] Division of Genetics, Department of Medicine, Brigham and Women's Hospital and Harvard Medical School, Boston, MA, USA

[2] T. H. Chan School of Public Health, Harvard University, Boston, MA, USA

[3] Massachusetts College of Pharmacy and Health Sciences, Boston, MA, USA

[4] Department of Pharmacy, Massachusetts General Hospital, Boston, MA, USA

[5] University Center for Primary Care and Public Health, University of Lausanne, Lausanne, Switzerland

[6] Department of Computational Biology, University of Lausanne, Switzerland

[7] Swiss Institute of Bioinformatics, Lausanne, Switzerland

[8] Altos Labs, San Diego, CA, USA

[9] Departments of Human Genetics and Biostatistics, University of California, Los Angeles, CA, USA

[10] Department of Genetics, School of Medicine, Stanford University, Stanford, CA, USA

[11] Center for Intelligent Medicine Research, Greater Bay Area Institute of Precision Medicine (Guangzhou), Fudan University, Guangzhou, China

[12] State Key Laboratory of Genetic Engineering, Center for Evolutionary Biology, School of Life Sciences, Fudan University, Shanghai, China

[13] Department of Medical Epidemiology and Biostatistics, Karolinska Institutet, Stockholm, Sweden

[14] Centre for Global Health Research, Usher Institute, University of Edinburgh, Edinburgh, UK

email: vgladyshev@rics.bwh.harvard.edu

Abstract

Machine learning models based on DNA methylation data can predict biological age but often lack causal insights. By harnessing large-scale genetic data through epigenome-wide Mendelian Randomization, we identified CpG sites potentially causal for aging-related traits. Neither the existing epigenetic clocks nor age-related differential DNA methylation are enriched in these sites. These CpGs include sites that contribute to aging and protect against it, yet their combined contribution negatively affects age-related traits. We established a novel framework to introduce causal information into epigenetic clocks, resulting in DamAge and AdaptAge—clocks that track detrimental and adaptive methylation changes, respectively. DamAge correlates with adverse outcomes, including mortality, while AdaptAge is associated with beneficial adaptations. These causality-enriched clocks exhibit sensitivity to short-term interventions. Our findings provide a detailed landscape of CpG sites with putative causal links to lifespan and healthspan, facilitating the development of aging biomarkers, assessing interventions, and studying reversibility of age-associated changes.

Main text

Introduction

Aging, a complex biological process, is characterized by the accumulation of deleterious molecular changes, leading to organ and system function decline and eventual death [1]. Although the underlying mechanisms of aging are not well understood, various studies indicate that aging is associated with altered DNA methylation patterns, particularly 5-methylcytosine (5mC) in mammals, where overall methylation slightly decreases in adulthood, but certain regions may experience hypo- or hypermethylation [2,3]. Specific CpG site methylation levels correlate strongly with age, enabling the development of machine learning-based epigenetic aging clocks (e.g., Horvath pan tissue and

Hannum blood-based clocks) that predict biological sample ages with high accuracy [4–6]. These clocks, more closely related to health measures than chronological age, are seen as better biological age indicators [7].

However, epigenetic aging clocks, primarily correlative, should be interpreted cautiously [8]. It remains unclear whether the DNA methylation differences used for age prediction are causal to aging-related phenotypes or merely aging byproducts. Establishing causality typically involves randomized controlled trials (RCTs), where treatment effects are assessed by comparing intervention and control groups, eliminating confounding factors [9,10]. But, given the genome's vast CpG sites, such individual perturbations are impractical.

Mendelian randomization (MR), a genetic causal inference approach, mimics RCT principles [11]. It uses genetic variants associated with exposure as instrumental variables, leveraging the natural random distribution of parental genome to offspring. MR has been applied to molecular traits using molecular quantitative trait loci (molQTLs), including DNA methylation (meQTL) [12]. Previous studies have successfully used meQTLs to identify causally linked CpG sites for diseases [13]. Integrating molQTLs with genome-wide association studies for aging-related traits allows for two-sample MR to estimate the molecular changes' causal effects on aging.

Here, we leveraged large-scale genetic data and performed epigenome-wide Mendelian Randomization (EWMR) on 420,509 CpG sites to identify CpG sites that are causal to eight aging-related traits. We found that none of the existing clocks are enriched for putative causal CpG sites. We further constructed a causality-enriched clock based on this inferred causal knowledge, as well as clocks that separately measure damaging and protective changes. Their applications provide direct insights into the aging process. Thus, our results offer a comprehensive map of human CpG sites causal to aging traits, which can be used to build causal biomarkers of aging and assess novel anti-aging interventions and aging-accelerating events.

Epigenome-wide MR on aging-related phenotypes

MR is an established genetic approach for causal inference that utilizes natural genetic variants as instrument variables [14]. Since the allocation of genetic variants is a random process and is determined during conception, the causal effects estimated using MR are not biased by environmental confounders. Therefore, it could be used as a tool for investigating causal relationships between

the DNA methylation and aging-related phenotypes (Fig. 1a). In the context of MR, a CpG site can be defined as causal when associations of SNPs with CpG methylation are directionally consistent and proportional in magnitude to its associations with aging-related phenotypes.

To identify CpG sites causal to aging, we used 420,509 CpG sites with meQTLs available (GoDMC, whole blood samples from 36 cohorts, 27,750 European subjects) as exposures and selected eight aging-related phenotypes as outcomes (Fig. 1a, Methods, Table 1), including two lifespan-related traits: lifespan and extreme longevity (defined as survival above 90th percentile) [15,16]; three health-related traits: healthspan (age at the first incidence of any major age-related disease) [17], frailty index (measurement of frailty based on the accumulation of a number of health deficits during the life course) [18], and self-rated health (based on the questionnaire responses) ; and three summary-level aging-related traits: Aging-GIP1 (the first genetic principle component of six human aging traits - healthspan, father's and mother's lifespan, exceptional longevity, frailty index and self-rated health) [19], socioeconomic traits-adjusted Aging-GIP1, and healthy aging (multivariate genomic scan of healthspan, lifespan, and longevity) [20].

Aging-GIP1 captures both the length of life and age-related health status, which can be considered as a genetic representation of healthy longevity. It also shows the strongest genetic correlation with all other traits related to lifespan [19]. Therefore, we further used Aging-GIP1 as the primary aging-related trait to investigate CpG sites causal to the aging process. A genetic correlation analysis showed that all eight lifespan- and health-related traits are genetically correlated and clustered with each other (Extended Data Fig. 1).

We then applied generalized inverse-variance weighted MR (gIVW) and MR-Egger (gEgger) to each exposure-outcome pair (Method). Post-Bonferroni correction, we identified over 6,000 significant causal CpG sites for each trait (Fig. 1c). The causal effect estimates across traits exhibited a strong correlation (Fig. 1d). To mitigate reverse causation, we conducted cis-reverse MR and Steiger directionality tests [21]. Additionally, to control false positives from MR due to linkage disequilibrium (LD) or pleiotropy, we also employed pairwise conditional and colocalization (PWCoCo) analysis (Fig. 1b, Method) [22]. Over half of the MR-identified CpG sites for each trait showed colocalized signals.

Given the analysis was limited to 420,509 CpG sites, the effects of unmeasured CpG sites on traits couldn't be differentiated. To validate whether MR-estimated effects can be attributed to single CpG sites, we analyzed naturally occurring point mutations at putative causal CpG sites (meSNP). Nearly 10% of CpG sites on the human methylation array have an meSNP, and we found significant depletion of meSNPs at causal sites, suggesting negative selection against loss-of-function mutations, likely due to causal site enrichment in regulatory regions (Extended Data Fig. 2). A significant positive correlation (Pearson's R = 0.4, P = 1e-4) was observed between outcomes estimated using single meSNPs and MR for causal CpG sites with available meSNPs (Extended Data Fig. 2). Thus, the MR-estimated causal effects could partially be ascribed to individual CpG sites, yet many without meSNPs, and their methylation levels being highly correlated with neighboring sites, suggest these sites tag causal regulatory regions.

To prioritize CpG sites for Aging-GIP1, we filtered MR signals using P value thresholds after Bonferroni correction and ranked them by causal effect magnitude and colocalization probability (PP.H4). Top pro-longevity CpG sites included cg12122041 (HTT) annd cg02613937 (TOMM40) while top sites limiting longevity were cg04977528 (HEY) and cg06286026 (GRK4). Additionally, cg19514613 at the APOE locus was significant for limiting longevity. Notably, lifespan effects at HTT and MAML3 loci were previously identified [19], and TOMM40 and APOE are linked to Alzheimer's disease and lifespan. Adjusting for socioeconomic status, cg06636172 at the FOXO locus emerged as the top pro-longevity CpG site (Fig. 1e).

Putative causal CpGs are enriched in regulatory regions

To further understand properties of the CpG sites identified as causal to each aging-related trait, we performed an enrichment analysis using 14 Roadmap annotations [23]. We found that the putative causal CpGs for most traits are enriched in promoters and enhancers while depleted in quiescent regions (Fig. 2a). Furthermore, these sites were enriched in CpG shores (Extended Data Fig. 3). We observed that the putative causal CpG sites for Aging-GIP1 are significantly more evolutionally conserved compared to non-causal CpGs, based on both functional genomic conservation scores (Learning Evidence of Conservation from Integrated Functional genomic annotations, LECIF) and the phastCons/phyloP scores across 100 vertebrate genomes [24] (Fig. 2b, c, Extended Data Fig. 4). Moreover, the absolute value of the estimated causal effect sizes showed significant positive correlations between all three conservative scores. These results suggest that the CpG sites

identified as causal for aging-related traits are more likely to be in functional genomic elements and more evolutionarily conserved.

It is well known that DNA methylation status may affect transcription factor (TF) binding . To understand the relationship between putative causal CpG sites and TFs, we performed a transcription factor binding site enrichment analysis (Fig. 2d). The CpG sites causal to Aging-GIP1 were significantly enriched in the binding sites of 63 TFs, including POLR2A, ZNF24, MYC, and HDAC1; while depleted in the binding sites of 19 TFs, including CTCF, CHD4, and BRD9 (Fig. 2d). In particular, POLR2A was among the top enriched TFs in 6 of 8 traits. POLR2A is the POLR2 subunit (RNA polymerase II), and previous research showed that epigenetic modifications can modulate its elongation and affect alternative splicing [25]. Our results imply that this mechanism is potentially a major contributor that mediates the effects of DNA methylation on aging. We further found that there were 3 TF-binding sites (BRD4, CREB1, and E2F1) enriched with CpG sites whose methylation levels promote healthy longevity (Aging-GIP1), and 4 TF-binding sites (HDAC1, ZHX1, IKZF2, and IRF1) enriched with CpG sites whose methylation levels decrease healthy longevity (Extended Data Fig. 4).

Since the putative causal CpGs are enriched in regulatory regions and TF binding sites, we further performed a mediation analysis to investigate whether the effect top CpG hits are mediated through gene expression. The mediation effects were estimated through multivariable MR including both DNA methylation and gene expression, which dissect significant CpG-phenotype causal effects ($\boldsymbol{\theta}_T$) into direct effects ($\boldsymbol{\theta}_D$) and indirect effects through transcript levels (Method) [26]. Among 2,255 putative causal CpGs applicable to the mediation analysis for Aging-GIP1, 1,000 had their effect mediated by a major transcript (with mediation proportion > 0.03, Fig. 2e). For example, we found that the 92% of the effect of cg11299964 on Aging-GIP1 is mediated through the expression of MAPKAP1, which is a key protein in the mTOR signaling pathway (Fig. 2e). We then performed a gene set enrichment analysis on GO and KEGG using the mediator genes for Aging-GIP1 (Fig. 2f). We found that the mediators are enriched in several aging-related pathways, including mTOR signaling (P = 0.0018) and autophagosome assembly (P = 5.4e-4, Fig. 2f).

We also examined the enrichment of putative causal CpG sites in phenome-wide EWAS signals obtained from the EWAS catalog [27]. The top enriched phenotypes included rheumatoid arthritis, HIV infection, nitrogen dioxide exposure, and maternal obesity (Extended Data Fig. 5).

Interestingly, none of these conditions is primarily caused by aging but instead increased risk of mortality. Therefore, our results suggest that the causal CpG sites for aging are enriched in conditions that cause accelerated aging, but not in conditions that are caused by aging, consistent with the previous study that suggests that differentially expressed genes reflect disease-induced rather than disease-causing changes [1].

Existing Epigenetic clocks lack aging-causal CpGs

One open question for epigenetic clocks is whether their clock sites are causal to aging and age-related functional decline. To answer this question, we collected seven epigenetic age models in humans, namely, the Zhang clock, PhenoAge, GrimAge, PedBE, HorvathAge, HannumAge, and DunedinPACE. We then performed an enrichment analysis of putative causal CpGs for all eight lifespan/healthspan-related traits for each clock. After correcting for multiple testing, none of the existing clocks showed significant enrichment for putative causal CpGs of any of the lifespan/healthspan-related traits (Fig. 3g). PhenoAge showed a nominal significant enrichment with CpGs causal to healthspan and healthy aging, but it was not robust to the choice of thresholds. This finding suggests that, although some clocks contain CpGs causal to aging (Table 2), they, by design, favor CpG sites with a higher correlation with age and thus are not enriched with putative causal CpGs.

Identify protective and deleterious DNAm changes in aging

Another important question in epigenetic aging is the identity and number of epigenetic changes that (i) contribute to age-related damage and (ii) respond to it [30]. We approached this question by integrating information on the causal effect and age-related differential methylation for each CpG. The protective or damaging nature of age-related differential methylation at each CpG is indicated by the product of the causal effect and age-associated differential methylation ($b_{age} \times b_{MR}$, Fig. 4a). For example, if a higher methylation level of a certain CpG site leads to a longer lifespan or healthspan, then during aging, a decrease of the methylation level at that site would be considered as having a damaging effect, whereas an increased methylation level would be considered as having a protective effect.

The effect of DNA methylation estimated by MR is estimated through linear regression, which assumes that the relationship between DNA methylation level and lifespan-related outcome is

linear. Prior to annotating protective and damaging CpGs, it is important to make sure the effect size of genetic instruments on DNA methylation levels is in the same order of magnitude as the effect of aging. We show that the effect of genetic instruments is comparable with the effect of aging by calculating the ratio between the effect of strongest cis-meQTL and age-related differential methylation for each CpG site (Extended Data Fig. 6). The median ratio is 21.8 for all significant age-associated sites and 3.9 for top 50 age-associated sites, suggesting that the median effect of genetic instruments is roughly equivalent to the effect of years of aging.

Therefore, using the age-related blood DNA methylation data estimated from 7,036 individuals (ages of 18 and 93 years, Generation Scotland cohort)[31], we separated the CpG sites causal to eight traits related to lifespan into four different categories: protective hypermethylation, deleterious hypermethylation, protective hypomethylation, and deleterious hypomethylation (Fig. 4b, Extended Data Fig. 7). Among the top 10 CpG sites whose differential methylation during aging has a relatively large impact on healthy longevity, six hypermethylated CpG sites during aging exhibit strong protective effects, including cg18327056, cg25700533, cg19095568, cg17227156, cg17113968, and cg07306253; while one hypomethylated CpG site (cg04977528) also has a protective effect. In contrast, one hypermethylated CpG site (cg26669793) and two hypomethylated CpG sites (cg25903363 and cg26628907) show damaging effects (Fig. 4b).

Contradicting the popular notion that most age-related differential methylation features are bad for the organism, our findings revealed that, in terms of the number of CpGs, there was no enrichment for either protective or damaging differential methylation during aging (Extended Data Fig. 8). Note that the age-associated CpG sites are identified in cross-sectional studies, therefore, a fraction of protective sites we observed could be explained by survival bias (i.e., CpG sites that promote late-life survival). Interestingly, there is a stronger depletion of meSNP in adaptive sites compared to the damaging sites, consistent with the notion that the adaptative mechanism is stronger regulated compared to the damage (Extended Data Fig. 2) [30]. We also found that there was no significant correlation between the size of the causal effect and the magnitude of age-associated differential methylations (Fig. 4b, Extended Data Fig. 8), suggesting that CpG sites with a greater effect on healthy longevity do not necessarily change their level of methylation during aging. This result is consistent with our findings discussed above and explains the lack of enrichment of causal sites in existing epigenetic clocks.

The product of the causal effect and age-associated differential methylation ($b_{age} \times b_{MR}$) provides an estimate of the effect of age-related differential methylation on aging-related phenotypes in a unit of time. We calculated the cumulative effect of age-associated differential methylations on Aging-GIP1 by cumulative summing the effect of top 3,000 age-associated CpG sites, and calculated the empirical P-value through 10,000 permutations (Fig. 4c). Importantly, we discovered that although the number of protective and damaging CpG sites was similar, the cumulative effect of combined age-related DNA differential methylation is significantly detrimental to age-related phenotypes (P = 0.007), consistent with the overall damaging nature of aging.

Developing causality-enriched epigenetic clocks

Although various existing epigenetic aging clock models can accurately predict the age of biological samples, they are purely based on correlation. This means that the reliability of existing clock models is highly dependent on the correlation structure of DNA methylation and phenotypes. This may result in unreliable estimates when extrapolating the model to predict the age of novel biological conditions (i.e., applying clocks to interventions that do not exist in the training population), as the correlation structure may be corrupted by the new intervention.

To overcome this problem, we developed novel epigenetic clocks that are based on putative causal CpG sites identified by EWMR (Fig. 5a). Specifically, we trained an elastic net model predicting chronological age on whole blood methylation data from 2,664 individuals [31], using CpG sites identified as causal to adjusted Aging-GIP1 by EWMR (adjusted $P < 0.05$). In regular epigenetic clock models, the penalty weight is defined to be 1 for all CpG sites, which produces models that are purely based on correlation. Instead, we introduced a novel causality-enriched elastic net model, where we assigned the feature-specific penalty factor based on the causality score for each CpG site (Method). The influence of the causality score on the feature-specific penalty factor is controlled by the causality factor τ, which is an adjustable parameter. We also constructed the model in the way that the CpGs that promotes healthy longevity are favored (i.e., with $\beta > 0$), to avoid including sites that disrupt the system but unrelated to aging. If $\tau = 0$, the whole model is reduced to a regular elastic net regression, where the penalty factor equals one for all features. When τ becomes large, the model is more influenced by the causality score and tends to assign larger coefficients to the features with a higher causality score (Fig. 5A, Method).

Using this method, we trained the model to build the causality-enriched epigenetic clock CausAge (586 sites) using 2,664 blood samples. To separately measure adaptive and damaging DNA differential methylation during aging, we further separated putative causal CpG sites into two groups based on the causal effect size from MR and the direction of age-associated differential methylation (Fig. 4b). We then built DamAge, the damaging clock, which contains only the damaging CpG sites (1090 sites), and AdaptAge, the protective clock, which contains only the adaptive/protective CpG sites (1000 sites, Fig. 5a). We show that the model's accuracy significantly decreased as the causality factor τ increased (Fig. 5b, c, Extended Data Fig. 9). This is because the causality factor τ controls the trade-off between the correlation and causality score-weighted penalty factor, and the causality score is not always correlated with the predictive power of age. For example, a CpG site with a high correlation with age may not be causal to aging, and *vice versa*. We therefore selected causality factor τ of 0.3 in the downstream analysis, which is the largest τ value with MAE < 5 years in the validation set and maximized the association with mortality (Fig. 5c-d).

DamAge and AdaptAge uncouple damage and adaptation in aging

By design, AdaptAge contains only the CpG sites that capture protective effects against aging. Therefore, in theory, the subject predicted to be older by AdaptAge may be expected to accumulate more protective changes during aging. On the contrary, DamAge contains only the CpG sites that exhibit damaging effects, which may be considered as a biomarker of age-related damage. Therefore, we hypothesized that DamAge acceleration may be harmful and shorten life expectancy, whereas AdaptAge acceleration would be protective or neutral, which may indicate healthy longevity.

To test this hypothesis, we first analyzed the associations between human mortality and epigenetic age acceleration quantified by causality-enriched clocks using 4,651 individuals from the Framingham Heart Study, FHS offspring cohort (n = 2,544 Caucasians, 54% females, Supplementary Information) and Normative ageing study (NAS, n = 2,280, Supplementary Information). Among the three causality-enriched clocks, DamAge acceleration showed the strongest positive association on mortality (P = 9.9e-12) and outperformed CausAge (P = 0.01), AdaptAge (P = 0.008), Horvath clock (P = 0.34), Hannum clock (P = 8.2e-7), and is comparable to PhenoAge (P = 9.2e-11, Fig. 5d). This finding supports the notion that age-related damage is the main contributor to the risk of mortality, and the solely damage-base clock is better than the mixture of both damage

and adaptation. In contrast, AdaptAge acceleration showed a significant negative association with mortality, suggesting that protective adaptations during aging, measured by AdaptAge, are associated with longer lifespan. In addition, epigenetic age accelerations measured by DamAge and AdaptAge were near-independent (Pearson's R = 0.14, Extended Data Fig. 9). These findings highlight the importance of separating adaptive and damaging age-associated differential methylation when building aging clock models.

Interestingly, although the clock accuracy monotonically decreased as the causality factor τ increased, the association between mortality and epigenetic age acceleration did not follow the same trend (Fig. 5d). Especially for DamAge, the mortality association increased as the τ increased and peaked when τ was around 0.3. Also, DamAge consistently outperformed CausAge in predicting mortality risk, even though CausAge was more accurate in age prediction (Fig. 5b-e), the association between CausAge and mortality may be weakened due to the inclusion of adaptive sites. This suggests that although the introduction of the causality score and separation of damaging CpGs may decrease the accuracy of the clock in terms of predicting chronological age, it improves the prediction of aging-related phenotypes.

Induced pluripotent stem cell (iPSC) reprogramming is one of the most robust rejuvenation models, which was shown to be able to strongly reverse the epigenetic age of cells [32]. We applied the causality-enriched clock models to reprogramming of fibroblasts to iPSC [33]. For comparison, we also included five published epigenetic models, namely Horvath Age, Hannum Age, PhenoAge, GrimAge and DunedinPACE. The Horvath and Hannum clock were trained on chronological age [32,34], PhenoAge was trained on the age-adjusted by health-related phenotypes [35], GrimAge was trained on mortality [36], and DunedinPACE was trained to predict the pace of aging [37]. Consistent with Horvath clock, Hannum clock, PhenoAge, and GrimAge, DamAge revealed that epigenetic age decreased during iPSC reprogramming, but with a stronger negative correlation with the time of reprogramming and higher statistical significance (R = -0.93, P = 4e-12, Fig. 5f). This observation suggests that DamAge may better capture the damage-removal effect of iPSC reprogramming. On the contrary, AdaptAge increased significantly during the reprogramming process (R = 0.86, P = 1.3e-8), suggesting that protective age-associated differential methylation does not capture the rejuvenation effect and that in fact cells may acquire even more protective changes during iPSC reprogramming.

To further examine how DamAge and AdaptAge capture age-related damage and protective adaptations, respectively, we tested the performance of causality-enriched clocks using various datasets. We first examined several aging-related conditions, namely atherosclerosis, cancer, and hypertension (Fig. 6a). We analyzed the blood samples from clinical atherosclerosis patients (n = 8) and healthy donors (n = 8) in the LVAD study [38]. All eight clocks tested showed that the atherosclerosis patients are significantly older than healthy controls (Fig. 6a). We also analyzed 70 prostate cancer cases with good or poor prognosis [39]. Only DamAge successfully detected a significant age acceleration in patients with bad cancer prognosis (P = 0.039), while Hannum age detected a significant inverse effect where the patients with good prognosis were age accelerated (P = 0.044). For hypertensive heart disease, we analyzed blood samples from 44 hypertensive patients and 44 healthy controls [40]. Both CausAge and DamAge showed significant age acceleration in hypertensive patients (CausAge P = 0.002, DamAge P = 0.04). Similar effects could be detected with GrimAge (P = 0.002) and DunedinPACE (P = 0.02), but not with AdaptAge, PhenoAge, and two 1st generation clocks. These results suggest that DamAge could more robustly represent the effect of age-related conditions, compared to the published 1st and 2nd generation clocks.

Next, we examined conditions that specifically promote age-related damage (Fig. 6b). Smoking is a well-known risk factor for many age-related diseases, and it also causes DNA damage and oxidative stress. We compared the epigenetic age of smokers (n = 40) and non-smokers (n = 40) [41]. CausAge (P = 0.004) and DamAge (P = 0.006), together with all three 2nd generation clocks could detect significant age-acceleration among smokers, while AdaptAge and two 1st generation clocks did not. Progeroid syndrome is a group of rare genetic disorders that cause premature aging. We analyzed blood cell samples from healthy donors (n = 3), and patients with Hutchinson-Gilford Progeria Syndrome (HGP, n = 3) and Werner Syndrome (n = 4) [42]. We observed significant DamAge acceleration in both HGP (P = 0.004) and Werner Syndrome (P = 5e-4) compared to healthy controls. Similar effects were detected also with PhenoAge and GrimAge. Hannum age and DunedinPACE detected age acceleration in Werner Syndrome but not in HGP, while no significant effect was found by other clocks (Fig. 6b). We then analyzed dermis and epidermis samples with or without sun exposure (n = 10 per group) in old adults (age > 60) [43]. As the exposure to ultraviolet promotes DNA damage and aging, it may be considered a model of age-related damage. As expected, we observed significant DamAge acceleration in sun-exposed epidermis compared to sun-

protected epidermis (P = 2e-5), while no significant effect was observed in the dermis tissue. AdaptAge of the sun-exposed epidermis was significantly lower (P = 0.01). Surprisingly, based on most other published clocks (including Horvath age, Hannum age, and DunedinPACE), the sun-exposed epidermis was predicted to be significantly younger than sun-protected epidermis. Only GrimAge showed the expected effect direction but did not reach statistical significance (P = 0.1).

Paraoxonase 1 (PON1) is one of most studied genes associated with cardiovascular disease, oxidative stress, inflammation, and healthy aging . Specifically, PON1 plays an important role in detoxifying organophosphorus compounds and removing harmful oxidized lipids [44]. The genetic variant of PON1 (R192Q) significantly decreases PON1 activity and is known to be associated with an increased risk of cardiovascular disease and neurodegenerative diseases [45]. Interestingly, the PON1 Q allele is significantly depleted in centenarians [45]. We analyzed the relationship between PON1 activity and epigenetic age in 48 whole blood samples (Fig. 6a) [46]. DamAge shows a significant negative correlation with PON1 activity (R = -0.55, p = 0.0062), whereas AdaptAge showed a significant positive correlation with PON1 activity (R = 0.69, p = 0.0003). Again, this association was not observed by other epigenetic clocks, except for Horvath age, but with a less significant negative correlation (P = 0.04). Together, we showed that DamAge can reliably detect damage-related biological age acceleration.

Causality-enriched clocks could also capture the aging-related effects of short-term interventions. We first examined the effect of human umbilical cord plasma concentrate injection, which was reported to have age reversal effects [47]. In this study, 18 older participants were treated with human umbilical cord plasma concentrate injection weekly (1 ml intramuscular) over a 10-week period. We found that this rejuvenation effect could only be captured with DamAge (P = 0.04) and GrimAge (P = 0.04, Fig. 6c). Note that this effect is not detected by other clocks, including AdaptAge, which may be contributed by the weak effect and short treating interval. Similarly, a 6-week omega-3 fatty acid supplementation in overweight subjects (n = 34) [48], which was shown to be protective against age-related cardiovascular diseases, significantly increased AdaptAge (P = 0.009) and reduced DamAge (P = 0.02, Fig. 6c). We also found that short-term treatment with cigarette smoke condensate in bronchial epithelial cells significantly accelerated DamAge (P = 0.002) but did not affect other tested clocks (Fig. 6c). Together, our data demonstrate the

375 importance of separating damage and adaptation when building biomarkers of aging and provide
376 novel tools to quantify aging and rejuvenation.

377 Small for gestational age (SGA) is a condition defined as birth weight less than the 10th percentile
378 for gestational age, usually due to limited access to the nutrient. We found that children with SGA
379 have a significantly lower DamAge and higher AdaptAge than children with normal birth weight
380 (GSE47880, Extended Data Fig. 10). These effects were not captured by other epigenetic clocks
381 tested. SGA is usually considered a pathological condition; some studies suggest that it may be
382 because early life benefits can be reversed in later life by exposure to excess nutrients. The differ-
383 ent roles of SGA in the early and late stages of life may need to be further investigated in future
384 studies.

385 In vitro fertilization (IVF) is a common method of treating infertility. Yet, previous studies have
386 shown that IVF may increase the risk of perinatal morbidity and mortality. We analyzed the DNA
387 methylation data from neonatal blood spots of 137 newborns conceived unassisted (NAT), through
388 intrauterine insemination (IUI), or through IVF using fresh or cryopreserved (frozen) embryo
389 transfer [49]. We found that IVF-conceived newborns using fresh or cryopreserved embryos had
390 higher DamAge acceleration and lower AdaptAge than NAT-conceived newborns (Extended Data
391 Fig. 10). On the other hand, IUI-conceived newborns showed no differences in their DamAge and
392 AdaptAge with controls (Extended Data Fig. 10). This effect could not be observed by other five
393 epigenetic clocks tested, except for Horvath age. We also analyzed peripheral blood DNA meth-
394 ylation data from patients with single-locus or Multi-loci imprinting disturbances (SLID or MLID),
395 which is the condition of losing methylation at single or multiple imprinting centers [50]. Similar to
396 IVF, we found that patients with imprinting disorders showed significantly higher DamAge and
397 lower AdaptAge (Extended Data Fig. 10). Together, these results suggest that DamAge and
398 AdaptAge may serve as preferred biomarkers for the events affecting aging traits during develop-
399 ment.

400 **Discussion**

401 Epigenetic aging clocks, like those based on DNA methylation patterns, are adept at predicting the
402 age of biological samples [8]. DNA methylation changes with age, influencing chromatin structure
403 and gene expression, potentially affecting aging phenotypes. For instance, DNA methylation may
404 play a causal role in cellular rejuvenation during iPSC reprogramming [32]. However, it's crucial to

discern if age-related differential DNA methylation causes aging phenotypes or merely the downstream effect of them. Transcriptome-wide Mendelian Randomization (MR) studies suggest that differentially expressed genes in diseases often result from, rather than cause, the disease [28]. Our epigenome-wide MR (EWMR) supports this, showing minimal overlap between CpG sites causally linked to healthy longevity and those changing with age.

MR is a powerful method to identify causal relationships between exposure traits and phenotypes [14]. The causality between the exposure and outcome in MR studies relies on three key assumptions: First, the genetic variants used as instrumental variables (IVs) must be robustly associated with the exposure of interest. Second, the IVs should not be associated with any confounding factors that influence both the exposure and the outcome. Third, the association between the IVs and the outcome must be mediated solely through the exposure, not through any alternative pathways. In our study, we used SNPs associated with DNA methylation levels at specific CpG sites as IVs to investigate their causal relationship with aging-related outcomes. While MR provides a framework to infer causality, it is crucial to recognize its limitations, particularly in the context of complex traits like aging. Our approach, although comprehensive, does not definitively establish causality but rather suggests putative causation based on the MR framework. The assumption that the effect of SNPs on aging-related outcomes is mediated exclusively through methylation changes at CpG sites is challenging to validate and may not encompass all underlying mechanisms. Hence, while our results contribute to the understanding of the relationship between DNA methylation and aging, they should be interpreted with caution, recognizing inherent limitations of the MR approach in fully elucidating causal pathways in the complex landscape of aging biology.

MR is also limited by the availability of genetic instruments for those traits [14]. In our study, we used DNA methylation quantitative trait loci (meQTLs) from the Illumina 450K array as instruments. But, the high correlation between nearby CpG sites and the scarcity of mutations at causal CpG sites (meSNPs) make it challenging to separate individual CpG effects. Hence, identified CpG sites are more likely markers for causal regions in aging-related phenotypes. While our findings mainly pertain to blood, as our genetic instruments were derived from the largest meQTL study in blood (GoDMC), a significant proportion of cis-meQTLs are tissue-conserved, suggesting broader relevance [50].

Considering molecular changes in aging for intervention targets may be flawed, as correlation doesn't imply causation. Many molecular changes could be neutral or adaptive responses to aging. For example, declines in IGF-1 and growth hormone, and increased protein aggregation in C. elegans, are adaptive mechanisms extending lifespan [43,51]. Our results indicate such adaptations at the epigenetic level are as common as damaging changes. Hence, focusing on causal effects and their direction is crucial.

Our causal epigenetic clock models (CausAge, AdaptAge, DamAge) distinguish protective changes from damaging ones. AdaptAge, for instance, predicts lower mortality risk in individuals with elevated protective adaptations. Interestingly, DamAge and AdaptAge, while accurately predicting chronological age, reflect different biological meanings in their delta-age terms. Their correlation in the general population may stem from survival and collider biases, highlighting the need for careful interpretation of epigenetic age acceleration in clinical settings.

In conclusion, our causality-enriched clock models offer new insights into aging mechanisms and the evaluation of interventions. They underscore the importance of distinguishing between adaptive and damaging epigenetic changes in aging research. Future studies, especially in diverse tissues, are needed to expand and validate these findings.

Methods

The research conducted in this study adheres to all applicable ethical regulations. This study, due to its nature, did not require ethical review or approval by an institutional review board.

Epigenome-wide Mendelian Randomization analysis

In MR analysis, the definition of causal relationship is that associations of SNPs with CpG methylation are directionally consistent and proportional in magnitude to associations of SNPs with aging-related phenotypes. Genetic variants that are strongly associated with whole blood DNA methylation level (FDR < 0.05) were used for the MR analysis. Only meQTLs in the cis-acting regions were used to avoid pleiotropic effects. As the generalized MR method achieves a higher statistical power by including partially correlated instruments while accounting for the LD structure, we used LD clumping to only remove meQTLs with strong LD ($r^2 > 0.3$), as suggested by Burgess et al. [52]. Three MR methods were used for the main analyses: Wald ratio when only one

meQTL was available, generalized inverse variance weighted (gIVW) when at least two meQTLs were available, and generalized MR-Egger regression (gEgger) when at least three meQTLs were available [52]. The MR analyses were conducted using the MendelianRandomization R package and TwoSampleMR R package [53,54].

We only included cis-meQTLs (meQTLs located within 2 MB of target CpG sites) in our analysis to avoid pleiotropic effects, as they are more likely to affect DNA methylation via direct mechanisms. To remove additional pleiotropic effects, we used the results of gEgger, whose estimate is robust to directional pleiotropic effects if the significant intercept is detected by gEgger regression ($P < 0.05$).

CpG-phenotype pairs with $P_{\text{adjusted}} < 0.05$ after Bonferroni correction were used to select causal CpG sites with the strongest MR evidence. All CpG-phenotype pairs with FDR < 0.05 were considered potential causal CpG sites and used in the downstream sensitivity analysis.

Mediation analysis

We conducted multivariable MR (MVMR) to dissect significant CpG-phenotype causal effects ($\boldsymbol{\theta}_{\text{T}}$) into direct effects ($\boldsymbol{\theta}_{\text{D}}$) and indirect effects through transcript levels following the methodology outlined in Sadler et al., 2022 and using the smr-ivw software (https://github.com/masadler/smrivw)[26]. Genetic effect sizes on CpGs (mQTLs) came from the GoDMC consortium (N=32,851) [12], and on transcript levels (eQTLs) from the eQTLGen consortium (N=$31,684) [55], both derived from whole blood. Mediation analyses were assessed for CpG-Aging-GIP1 and CpG-adjusted Aging-GIP1 pairs.

Transcript mediators were selected to be in *cis* (< 500kb away from the CpG site) and causally associated to the CpG. This latter condition was satisfied when univariable MR effects from the CpG site on the transcript had an MR p-value < 0.01. Instrumental variants were required to be associated to either the CpG or included transcripts and as in the univariable MR analysis they were selected to be correlated at $r^2 \leq 0.3$. The mediation proportion (MP) was estimated as 1- $\hat{\theta}_{\text{D}}/\hat{\theta}_{\text{T}}$.

Causality-enriched epigenetic clock model

Elastic net regression is a regularized linear model that solves the problem.

$$\hat{\beta} = argmin\big(RSS(\beta) + \lambda J(\beta)\big)$$

where $RSS(\beta)$ is the residual sum of squares, λ is the regularization parameter, and $J(\beta)$ is the regularization term [56]. The $J(\beta)$ term is the sum of the L1 and L2 terms, which is defined as

$$J(\beta) = \alpha \sum_{f=1}^{p} w_f \left|\beta_f\right| + \frac{1}{2}(1-\alpha) \sum_{f=1}^{p} w_f \, \beta_f^2$$

The parameter is the elastic net mixing parameter, which controls the balance between the L1 and L2 terms. w_f is the penalty factor for each feature we introduced. In a regular epigenetic clock model, w_f is defined to be 1 for all the features, which produces the model that is purely based on correlation. We introduced a causality-enriched elastic net model, where we defined the feature-specific penalty factor as

$$w_f = \frac{p s_f}{\sum_{f=1}^{p} s_f}$$

$$s_f = \big(\max(c_f) + min(c_f) - c_f\big)^{\tau}$$

Here the c_f is the absolute value of the causality score for each feature, which is calculated from the causal effect size from MR weighted by colocalization probability. The $\tau > 0$ is a tuneable parameter that controls how much the causality score affects the feature-specific penalty factor. If $\tau = 0$, the whole model is reduced to a regular elastic net regression, where $w_f = 1$ for all the features. When τ becomes large, the model is more influenced by the causality score and tends to assign larger coefficients to the features with a higher causality score. To balance the precision and causality, we defined τ as 0.3, which is the largest τ value with MAE < 5 years in the validation set and maximized the association with mortality. In addition, we introduced a hyperparameter array to control the limits of each model weight, ensuring the range and sign of the weight align with the patterns of aging. The upper limits for the sites that decrease healthy longevity are defined to be a small value (β of the site by default) to encourage the models rely more on CpG sites that promotes healthy longevity.

Using this method, we trained the model on whole-blood methylation data from 2,664 individuals [57]. We built the causality-enriched epigenetic clock model CausAge. To separately measure

515 adaptive and damaging DNA methylation changes during aging, we further separate the causal
516 CpG sites into two groups based on causal effect size from MR and the direction of age-related
517 changes. We then built DamAge, a damaging clock, and AdaptAge, a protective clock.

518 **Genetic correlation analysis**

519 Genetic correlation between traits related to aging is calculated using the LD score regression
520 (LDSC) [58]. SNPs that were imperfectly imputed with INFO less than 0.9 or with a low minor allele
521 frequency less than 5% were removed to reduce statistical noise. LDSC was performed using
522 LDSC software v1.0.1 (https://github.com/bulik/ldsc).

523 **Sensitivity analyses**

524 *Horizontal pleiotropy*. The horizontal pleiotropic effect in instrumental variants may cause biased
525 causal effect estimation from the gIVW method. To detect unbalanced horizontal pleiotropy
526 among genetic instruments, we used the intercept gEgger regression, which provides an estimate
527 of the directional pleiotropic effect [59]. Note that by including a partially correlated instrument, the
528 gEgger intercept also has more statistical power to detect the pleiotropic effect. CpG-phenotype
529 pairs with gEgger intercept *P* value less than 0.05 were potentially affected by the pleiotropic
530 effect, and the gIVW method may be biased. We, therefore, reported an estimate and *P* value from
531 the gEgger method instead of the gIVW method for these MR signals, as the gEgger estimate is
532 robust to the horizontal pleiotropic effect [59].

533 *Heterogeneity*. To detect heterogeneity of the MR estimates in each meQTL, we performed the
534 Cochran's Q test and the Rücker's Q test for the gIVW and gEgger results, respectively. Since
535 heterogeneity does not necessarily affect causal effect estimation, we kept the MR signals hetero-
536 geneous while reporting potential heterogeneity in the result table.

537 *Directionality test*. To exclude MR signals caused by reverse causality (i.e., methylation changes
538 caused by outcome phenotype), we applied MR Steiger test [21], which is the method to test the
539 directionality of causal effect estimated by MR. We then removed all MR signals with reverse
540 directionality. We also applied the cis-reverse MR on the CpG-outcome pairs if the genome-wide
541 significant instrument for the outcome traits is available. The CpG-outcome pairs with correct
542 causal effect direction and non-significant reverse causal effects are marked as with correct causal
543 direction.

544 *Colocalization analysis.* All MR signals that passed the FDR threshold of 0.05 were then subjected
545 to the colocalization analysis. We applied pairwise a conditional and colocalization (PWCoCo)
546 analysis [60], which is a powerful genetic colocalization approach that is able to detect multiple in-
547 dependent genetic signals. We considered colocalization probability (PP.H4) > 70% as strong ev-
548 idence of colocalization. Also, since aging-related GWAS are in general noisy while cis-meQTL
549 usually have strong genetic signals, colocalization probability tends to be low, and the probability
550 of only having a signal from meQTLs (PP.H1) tends to be high. To overcome bias due to imbal-
551 anced power between exposure and outcome traits, we considered a conditional colocalization
552 probability (conditional PP.H4 = PP.H4 / PP.H3+H4) by assuming that the aging-related trait al-
553 ways has genetic signals in the region when a significant MR signal is detected. We then also
554 reported CpG-phenotype pairs with conditional PP.H4 > 70% as a potentially colocalized signal.

555 **Mortality association analysis**

556 To evaluate our novel causal clocks for predicting all-cause mortality risk, we applied the clocks
557 to a large-scale dataset comprising 4,651 individuals from (a) the Framingham Heart Study, FHS
558 offspring cohort (n = 2,544 Caucasians, 54% females) [15,16] and (b) Normative ageing study (dbGaP
559 accession phs000853.v2.p2)[61]. Methylation levels were profiled in blood samples based on Illu-
560 mina 450k arrays. In FHS, the mean (SD) chronological age at the time of the blood draw was 66.3
561 (8.9) years old. During follow-up, 330 individuals died. The mean (SD) follow-up time (used for
562 assessing time-to-death due to all-cause mortality) was 7.8 (1.7) years. As noted, this AgeAccel
563 measure is independent of chronological age. Next, we applied Cox regression analysis for time-
564 to-death (as a dependent variable) to assess the predictive ability of our causal clocks for all-cause
565 mortality, using the AgeAccel measures. The analysis was adjusted for age at the blood draw and
566 adjusted for gender and batch effect in FHS. We combined the results across FHS and NAS cohorts
567 by fixed effect models weighted by case number. The meta-analysis was performed in the R met-
568 afor function.

569 **Statistics & Reproducibility**

570 The Methods and Extended Methods sections outline statistical approaches employed in this study
571 for data analysis. Data processing and analysis were primarily performed using R version 4.0.2,
572 except where noted. In t-tests performed, data distribution was assumed to be normal but this was
573 not formally tested. Given the nature of this study, predetermining sample sizes, randomizing

experiments, and blinding investigators to experimental conditions were not relevant or applicable. In the clock training step, the CpG sites with less than 90% coverage were excluded from the analysis during quality control.

Data Availability

All analyses in this study were conducted using publicly available data. The datasets used are listed in Table 1 and their respective URLs are: Longevity GWAS summary statistics: https://www.longevitygenomics.org/downloads. Parental lifespan GWAS summary statistics: https://datashare.ed.ac.uk/handle/10283/3209. Healthspan GWAS summary statistics: https://www.gwasarchive.org/. Frailty index GWAS summary statistics: https://figshare.com/articles/dataset/Genome-Wide_Association_Study_of_the_Frailty_Index_-_Atkins_et_al_2019/9204998. Epigenetic age acceleration GWAS summary statistics: https://datashare.ed.ac.uk/handle/10283/3645. GEO datasets GSE107143, GSE127985, GSE192918, GSE193795, GSE210245, GSE51954, GSE94876, GSE98056, GSE101673, GSE78773, GSE90117, GSE79257, GSE42865. Any other data generated in this study upon which conclusions are based are available in Supplementary Tables.

Code Availability

Mendelian Randomization analyses were conducted using the R package TwoSampleMR version 0.5.6: https://mrcieu.github.io/TwoSampleMR/; R package MendelianRandomization version 0.7.0: https://cran.r-project.org/web/packages/MendelianRandomization/index.html; Genetic correlation analysis was performed using: LDSC software v1.0.1: https://github.com/bulik/ldsc. Mediation analysis was performed using smr-ivw v1.0 https://github.com/masadler/smrivw. Colocalization analysis was performed using PWCoCo v1.0 https://github.com/jwr-git/pwcoco. Elastic net model was trained using glmnet v4.1 https://cran.r-project.org/web/packages/glmnet/index.html. Custom code used are available in Supplementary Information. Algorithm of CausAge, DamAge, and AdaptAge are available in Supplementary information, as well as ClockBase (www.clockbase.org) and bio-learn python package (https://bio-learn.github.io/) [62,63].

Acknowledgments

We thank the DNA Methylation Consortium (GoDMC) for releasing the summary statistics of meQTLs. We also thank Csaba Kerepesi, Marco Mariotti, Daniel L. McCartney, and Riccardo E. Marioni for their help and advice during the initial stages of this study. We specially thank Yin Fang for the artwork design. This study is supported by the National Institute on Aging, Impetus grants and the Michael Antonov Foundation. The Framingham Heart Study is funded by National Institutes of Health contract N01-HC-25195 and HHSN268201500001I. The US Department of Veterans Affairs (VA) Normative Aging Study is supported by the National Institute of Environmental Health Sciences (NIEHS) (R01ES015172, R01ES021733) as well as by the Cooperative Studies Program/ERIC, US Department of Veterans Affairs, and is a research component of the Massachusetts Veterans Epidemiology Research and Information Center (MAVERIC). Additional support to the VA Normative Aging Study was provided by the US Department of Agriculture, Agricultural Research Service (contract 53-K06-510).

Author Contributions

K.Y. initiated the study and performed data collection and analyses. V.N.G. supervised this research and provided funding. H.L., M.C.S., and A.T. were involved in data analysis. A.T.L., M.M., and S.H. contributed to data interpretation. Z.K. and X.S. assisted in methodology refinement and statistical analysis. All authors contributed to writing and revising the manuscript and approved the final version for publication.

Competing interest statement

K.Y. and V.N.G. are inventors on a patent application related to the research reported.

Tables

Table 1. Datasets used in this study

Dataset	Description
GWAS data	
meQTLs	meQTLs were obtained from the Genetics of DNA Methylation Consortium (GoDMC). DNA methylation levels were measured in whole blood samples from 36 cohorts, including 27,750 European subjects. 420,509 CpG sites were analyzed (Min et al.)[12].
Aging-GIP1	First genetic principal component of six human aging traits - healthspan, father and mother lifespan, exceptional longevity, frailty index and self-rated health, which captures both length of life and indices of mental and physical wellbeing (Timmers et al.) [19].
Aging-GIP1-adj	Aging-GIP1 adjusted for household income and socioeconomic deprivation, from the same GWAS study as above [19].
Healthy aging	The multivariate genomic scan of healthspan, lifespan, and longevity (Timmers et al.) [20].
Lifespan	GWAS of lifespan from 512,047 mothers and 500,193 fathers of European ancestry (Timmers et al.)[15].
Longevity	11,262 subjects of European ancestry with a lifespan above the 90th percentile as the case group and 25,483 control subjects whose age at the last visit was below the 60th percentile age (Deelen et al.) [16].
Healthspan	The age of the first incidence of any major age-related disease, including dementia, congestive heart failure, diabetes, chronic obstructive pulmonary disease, stroke, cancer, myocardial infarction, as well as the incidence of death. The GWAS of healthspan included 300,447 subjects of European ancestry from the UK Biobank cohort (Zenin et al.) [17].
Frailty index	Calculated based on the cumulative number of health deficits during aging. The frailty index GWAS included 164,610 UK Biobank participants aged 60-70 years and 10,616 Swedish TwinGene participants aged 41-87 years (Atkins et al.) [18].
Self-rated health	Self-rated health GWAS was based on questionnaire responses on a scale of 0-5 in UK Biobank cohort, downloaded from Pan-UKBB project.
GEO data	
GSE107143	This study conducted DNA methylation analyses of blood samples from atherosclerosis patients and healthy donors.
GSE127985	DNA methylation changes in prostate cancer cases and it's prognosis.
GSE192918	This study analyzed peripheral whole blood DNA methylation profiles of pregnant women at different stages of gestation and post-delivery, identifying changes in DNA methylation patterns associated with different time points during pregnancy.
GSE193795	Genome-wide DNA methylation profiling was performed on 44 hypertensive and 44 healthy control samples, revealing distinct DNA methylation patterns associated with hypertension.
GSE210245	DNA methylation data from human whole blood samples were analyzed to assess the impact of treatment with human umbilical cord plasma concentrate injection.
GSE51954	Genome-wide DNA methylation profiling was conducted on epidermal and dermal samples obtained from sun-exposed and sun-protected body sites.
GSE94876	This study compared global methylation changes in buccal cells between smokers, moist snuff consumers, and non-tobacco consumers.
GSE98056	This study aimed to explore genome-wide DNA methylation changes and identify altered biological pathways resulting from n-3 fatty acid supplementation in overweight and obese individuals.
GSE101673	DNA methylation data for cigarette smoke condensate treated cell.
GSE78773	This study identified multi-locus methylation disturbances in individuals with different methylation patterns, including patients with Temple and Angelman syndromes
GSE90117	This study identified the relationship between PON1 activity, allele, and DNA methylation.
GSE79257	This study analyzed DNA methylation in infants born through different assisted reproductive techniques and unassisted conception, utilizing archived Guthrie cards for methylation profiling.
GSE42865	This study analyzed DNA methylation in B cells from patients with Hutchinson-Gilford Progeria Syndrome (HGP) and Werner Syndrome and controls.

627

628 **Table 2.** Putative causal CpG sites in existing epigenetic clocks. P values are adjusted for multiple
629 testing using Bonferroni's method.

	Position	Weight	outcome	Beta	SE	P	H4	role
HorvathAge (353)	cg06557358	-0.14	Overall_health_rating	-0.04	0.008	1.96E-07	0.89	Protective
	cg09509673	0.01	Healthy-aging	0.02	0.003	3.86E-13	0.85	Protective
	cg09509673	0.01	Lifespan	0.05	0.006	9.92E-20	0.83	Protective
	cg11299964	-0.16	Aging-GIP1	0.08	0.012	5.42E-12	0.86	Deleterious
	cg16744741	-0.35	Aging-GIP1	0.09	0.017	1.86E-08	0.89	Deleterious
	cg16744741	-0.35	Overall_health_rating	0.06	0.008	6.10E-14	0.86	Deleterious
PhenoAge (513)	cg05087948	-6.99	Aging-GIP1-adj	-0.08	0.013	7.30E-10	1.00	Protective
	cg21926612	-2.15	Overall_health_rating	0.01	0.002	3.27E-11	0.94	Deleterious
	cg11896923	-1.38	Healthspan	0.17	0.024	4.64E-12	0.90	Deleterious
	cg11896923	-1.38	Healthy-aging	0.05	0.008	5.63E-10	0.86	Deleterious
	cg00862290	-0.23	Healthy-aging	0.00	0.001	1.28E-08	0.85	Protective
	cg00862290	-0.23	Lifespan	-0.02	0.003	0	0.94	Protective
Zhang (514)	cg24987259	-1.33	Overall_health_rating	-0.04	0.007	8.25E-09	0.95	Protective
	cg05310309	0.18	Aging-GIP1	0.03	0.003	1.13E-32	0.96	Protective
	cg05310309	0.18	Overall_health_rating	0.01	0.002	2.64E-12	0.92	Protective
	cg06672696	0.02	Frailty-index	0.05	0.010	1.74E-07	0.82	Protective
PedBE (94)	cg04221461	0.03	Frailty-index	0.04	0.008	1.25E-07	0.95	Protective
	cg19381811	-0.08	Aging-GIP1	-0.04	0.004	3.26E-21	0.929544	Protective
	cg19381811	-0.08	Overall_health_rating	-0.03	0.002	8.80E-37	0.955032	Protective

630

631

632

Figure Legends

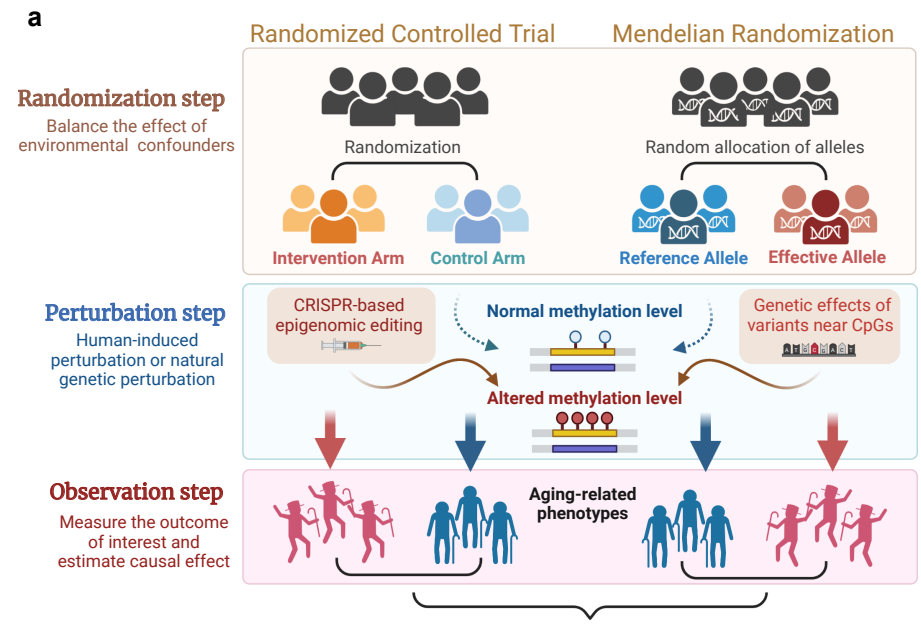
a
Randomized Controlled Trial
Mendelian Randomization
Randomization step
Balance the effect of environmental confounders
Randomization
Random allocation of alleles
Intervention Arm
Control Arm
Reference Allele
Effective Allele
Perturbation step
Human-induced perturbation or natural genetic perturbation
CRISPR-based epigenomic editing
Normal methylation level
Genetic effects of variants near CpGs
Altered methylation level
Observation step
Measure the outcome of interest and estimate causal effect
Aging-related phenotypes
Causal effect of DNA methylation on outcomes

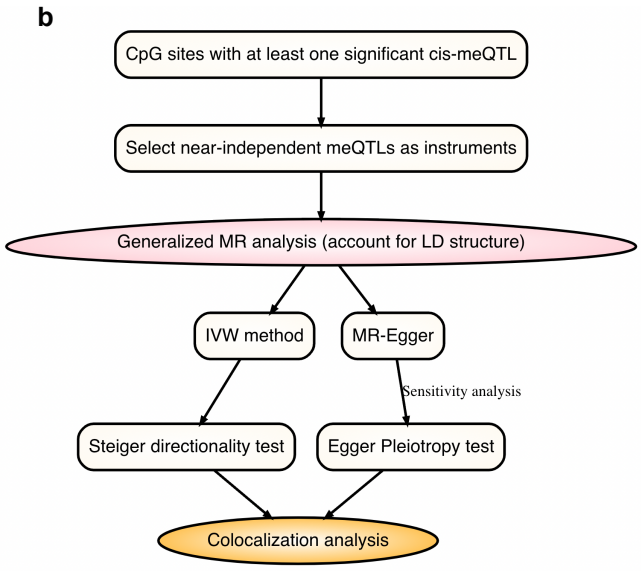
b
CpG sites with at least one significant cis-meQTL
Select near-independent meQTLs as instruments
Generalized MR analysis (account for LD structure)
IVW method
MR-Egger
Sensitivity analysis
Steiger directionality test
Egger Pleiotropy test
Colocalization analysis

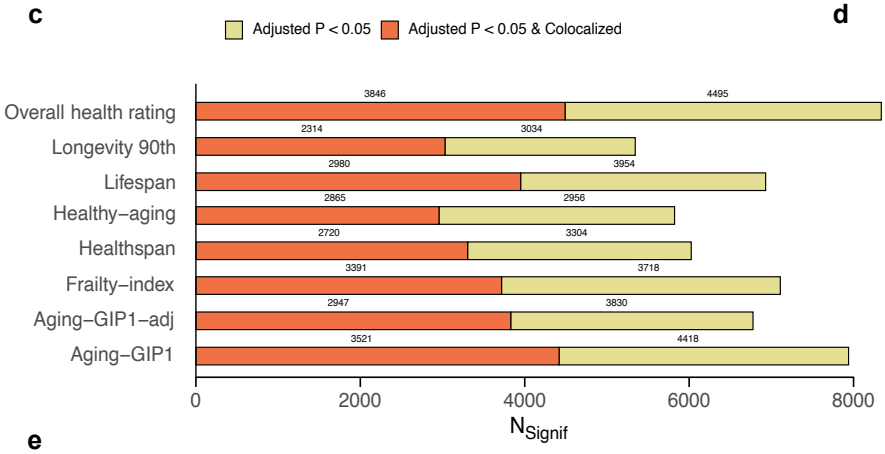
c
Adjusted P < 0.05
Adjusted P < 0.05 & Colocalized
Overall health rating
Longevity 90th
Lifespan
Healthy–aging
Healthspan
Frailty–index
Aging–GIP1–adj
Aging–GIP1
3846
4495
2314
3034
2980
3954
2865
2956
2720
3304
3391
3718
2947
3830
3521
4418
0
2000
4000
6000
8000
N_Signif

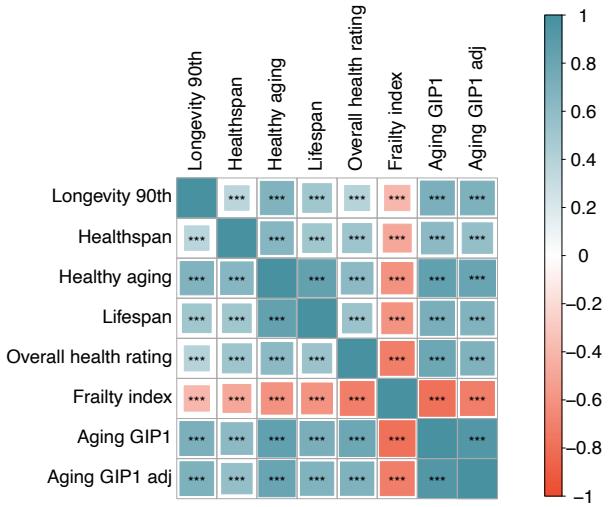
d
Longevity 90th
Healthspan
Healthy aging
Lifespan
Overall health rating
Frailty index
Aging GIP1
Aging GIP1 adj
1
0.8
0.6
0.4
0.2
0
−0.2
−0.4
−0.6
−0.8
−1

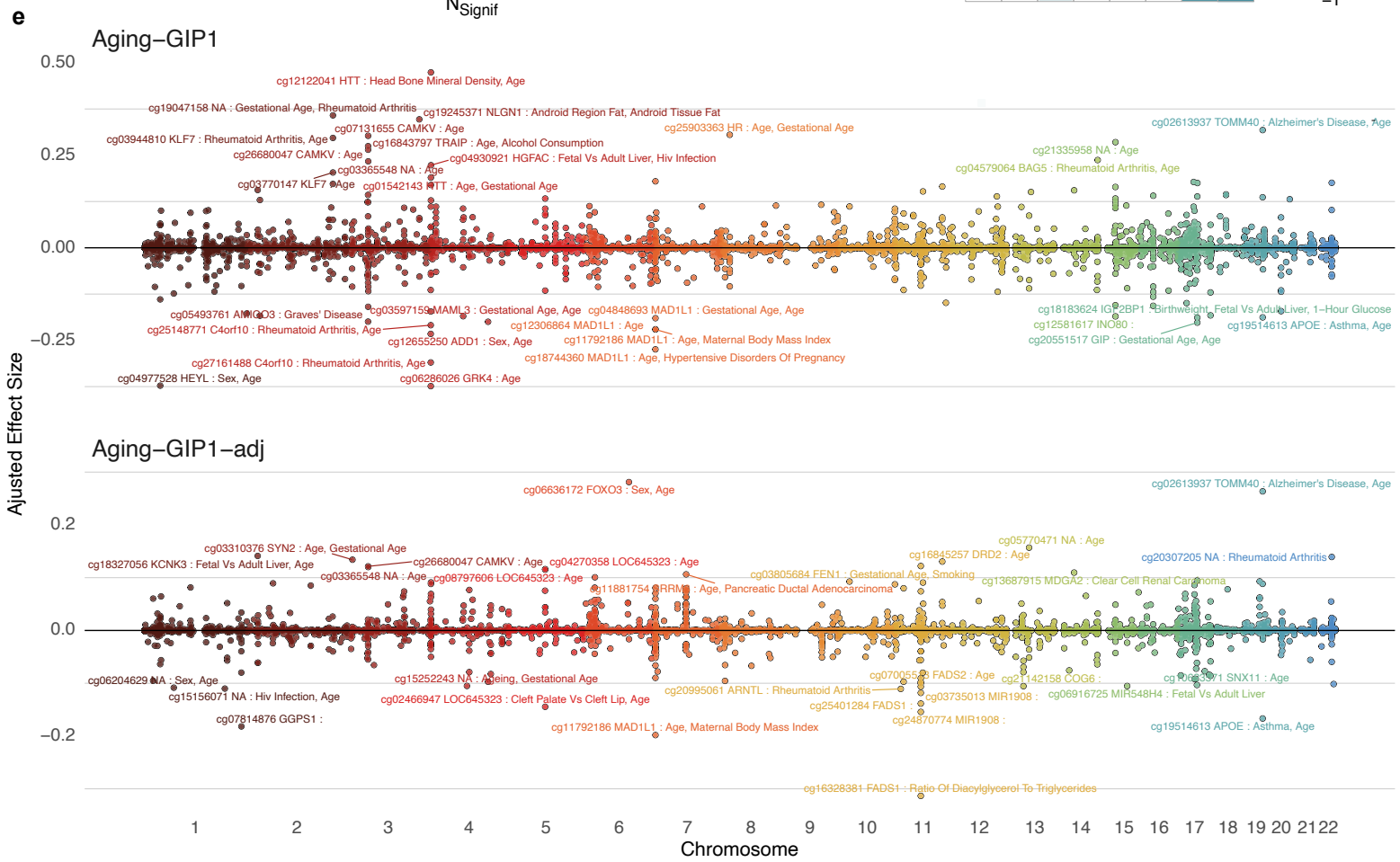
e
Aging–GIP1
Aging–GIP1–adj
Ajusted Effect Size
0.50
0.25
0.00
−0.25
0.2
0.0
−0.2
cg12122041 HTT : Head Bone Mineral Density, Age
cg19047158 NA : Gestational Age, Rheumatoid Arthritis
cg19245371 NLGN1 : Android Region Fat, Android Tissue Fat
cg25903363 HR : Age, Gestational Age
cg02613937 TOMM40 : Alzheimer's Disease, Age
cg03944810 KLF7 : Rheumatoid Arthritis, Age
cg07131655 CAMKV : Age
cg16843797 TRAIP : Age, Alcohol Consumption
cg26680047 CAMKV : Age
cg04930921 HGFAC : Fetal Vs Adult Liver, Hiv Infection
cg03365548 NA : Age
cg21335958 NA : Age
cg04579064 BAG5 : Rheumatoid Arthritis, Age
cg03770147 KLF7 : Age
cg01542143 HTT : Age, Gestational Age
cg05493761 AMIGO3 : Graves' Disease
cg03597159 MAML3 : Gestational Age, Age
cg04848693 MAD1L1 : Gestational Age, Age
cg18183624 IGF2BP1 : Birthweight, Fetal Vs Adult Liver, 1−Hour Glucose
cg25148771 C4orf10 : Rheumatoid Arthritis, Age
cg12306864 MAD1L1 : Age
cg12581617 INO80 :
cg19514613 APOE : Asthma, Age
cg12655250 ADD1 : Sex, Age
cg11792186 MAD1L1 : Age, Maternal Body Mass Index
cg20551517 GIP : Gestational Age, Age
cg27161488 C4orf10 : Rheumatoid Arthritis, Age
cg18744360 MAD1L1 : Age, Hypertensive Disorders Of Pregnancy
cg04977528 HEYL : Sex, Age
cg06286026 GRK4 : Age
cg06636172 FOXO3 : Sex, Age
cg02613937 TOMM40 : Alzheimer's Disease, Age
cg03310376 SYN2 : Age, Gestational Age
cg05770471 NA : Age
cg16845257 DRD2 : Age
cg20307205 NA : Rheumatoid Arthritis
cg18327056 KCNK3 : Fetal Vs Adult Liver, Age
cg26680047 CAMKV : Age
cg04270358 LOC645323 : Age
cg03365548 NA : Age
cg08797606 LOC645323 : Age
cg03805684 FEN1 : Gestational Age, Smoking
cg13687915 MDGA2 : Clear Cell Renal Carcinoma
cg11881754 RRM1 : Age, Pancreatic Ductal Adenocarcinoma
cg06204629 NA : Sex, Age
cg15252243 NA : Ageing, Gestational Age
cg07005528 FADS2 : Age
cg21142158 COG6 :
cg20995061 ARNTL : Rheumatoid Arthritis
cg03735013 MIR1908 :
cg06916725 MIR548H4 : Fetal Vs Adult Liver
cg15156071 NA : Hiv Infection, Age
cg02466947 LOC645323 : Cleft Palate Vs Cleft Lip, Age
cg25401284 FADS1 :
cg24870774 MIR1908 :
cg07814876 GGPS1 :
cg11792186 MAD1L1 : Age, Maternal Body Mass Index
cg19514613 APOE : Asthma, Age
cg16328381 FADS1 : Ratio Of Diacylglycerol To Triglycerides
1
2
3
4
5
6
7
8
9
10
11
12
13
14
15
16
17
18
19
20
21
22
Chromosome

637

638 **Fig. 1. Epigenome-wide Mendelian Randomization on various aging-related phenotypes. a.**
639 Schematic diagram shows the principle of MR using meQTLs as exposures and aging-related traits
640 as outcomes to identify putative causal CpG sites. **b.** Flow chart shows the procedure for epige-
641 nome-wide MR and sensitivity analysis. **c.** Number of significant putative causal CpG sites iden-
642 tified for each trait after adjusting for multiple comparisons using the Bonferroni correction. Red
643 regions of the bars indicate the number of putative causal CpG sites supported by the colocalization
644 analysis with conditional PP-H4 > 0.7. **d.** Spearman correlation of the estimated causal effects of
645 CpGs in twelve traits. *P* values reported are adjusted for multiple comparisons using Bonferroni
646 correction. Only CpGs with significant MR signals across at least six traits are included in the
647 analysis. Color scheme reflects Spearman correlation coefficients, * adjusted $P < 0.05$, ** adjusted
648 $P < 0.01$, *** adjusted $P < 0.001$. **e.** Modified Mississippi plot shows significant MR signals for
649 Aging-GIP1 and adjusted Aging-GIP1. Only the CpG sites adjusted for multiple comparisons with
650 FDR < 0.05 are shown in the plot. X-axis corresponds to the genomic positions of CpG sites; Y-
651 axis represents the size of the causal effect adjusted by colocalization probability (PP-H4). CpG
652 sites with top adjusted causal effects are annotated with the name and nearest gene. Only CpG sites
653 with adjusted $P < 0.05$ are included in the plot.

654

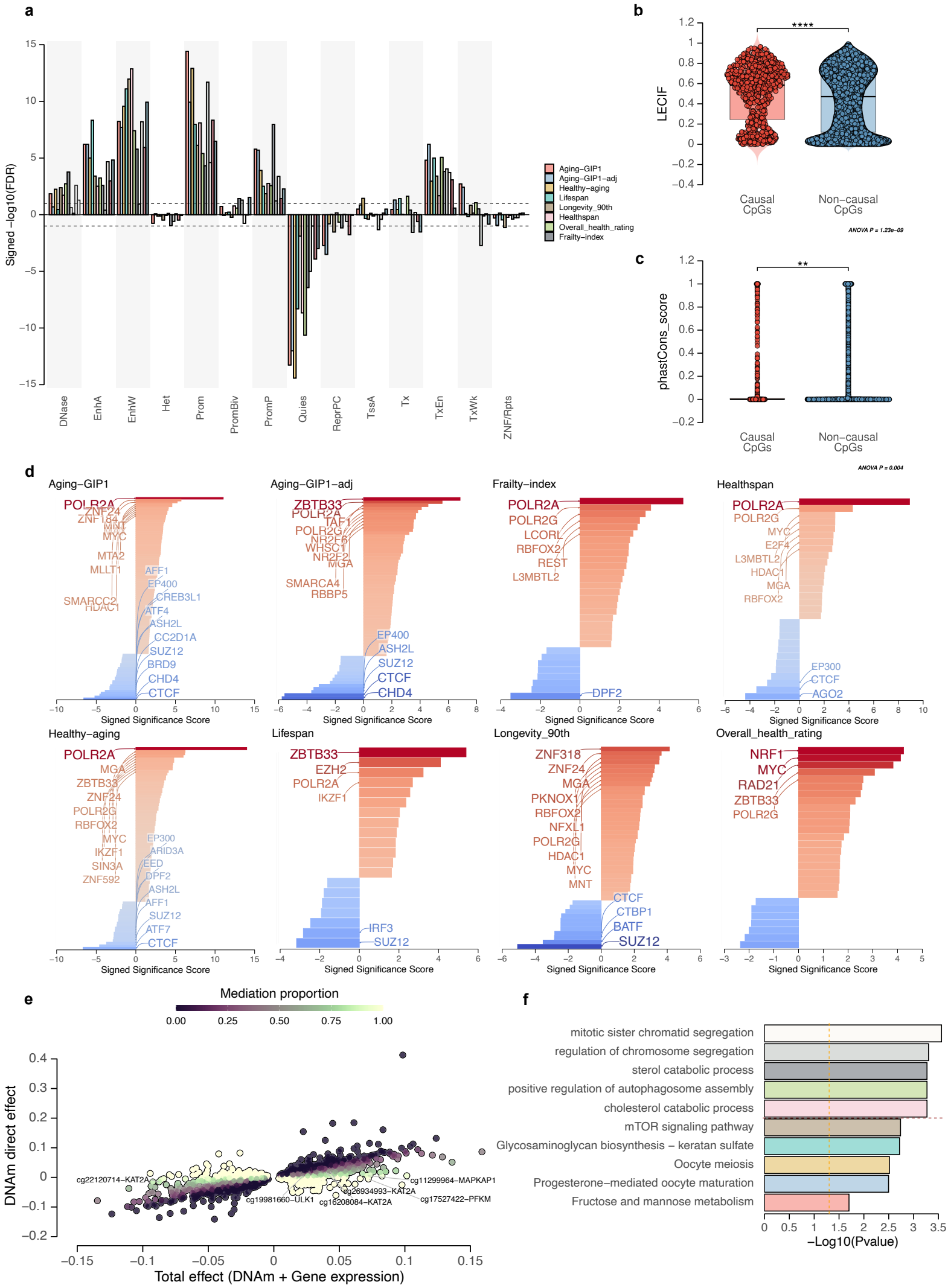
a
Signed −log10(FDR)
DNase
EnhA
EnhW
Het
Prom
PromBiv
PromP
Quies
ReprPC
TssA
Tx
TxEn
TxWk
ZNF/Rpts
Aging−GIP1
Aging−GIP1−adj
Healthy−aging
Lifespan
Longevity_90th
Healthspan
Overall_health_rating
Frailty−index
b
LECIF
****
Causal CpGs
Non−causal CpGs
ANOVA P = 1.23e−09
c
phastCons_score
**
Causal CpGs
Non−causal CpGs
ANOVA P = 0.004
d
Aging−GIP1
Aging−GIP1−adj
Frailty−index
Healthspan
Healthy−aging
Lifespan
Longevity_90th
Overall_health_rating
Signed Significance Score
e
Mediation proportion
DNAm direct effect
Total effect (DNAm + Gene expression)
cg22120714−KAT2A
cg19981660−ULK1
cg16208084−KAT2A
cg26934993−KAT2A
cg11299964−MAPKAP1
cg17527422−PFKM
f
mitotic sister chromatid segregation
regulation of chromosome segregation
sterol catabolic process
positive regulation of autophagosome assembly
cholesterol catabolic process
mTOR signaling pathway
Glycosaminoglycan biosynthesis − keratan sulfate
Oocyte meiosis
Progesterone−mediated oocyte maturation
Fructose and mannose metabolism
−Log10(Pvalue)

Fig. 2. CpG sites causal to aging are enriched in specific genetic regulatory regions. a. Bar plot shows enrichment of putative causal CpG sites in 14 Roadmap genomic annotations. Y axis shows -log10 (FDR) based on Fisher's exact test, signed by log2 (Odds ratio). Putative causal CpG sites identified for different traits are annotated with different colors. Two dotted horizontal lines show the FDR threshold of 0.05. TssA, active transcription start site. Prom, upstream/downstream TSS promoter. Tx, actively transcribed state. TxWk, weak transcription. TxEn, transcribed and regulatory Prom/Enh. EnhA, active enhancer. EnhW, weak enhancer. DNase, primary DNase. ZNF/Rpts, state associated with zinc finger protein genes. Het, constitutive heterochromatin. PromP, Poised promoter. PromBiv, bivalent regulatory states. ReprPC, repressed polycomb states. Quies, quiescent state. **b, c.** Box plot shows distribution of conservation scores in causal (n = 1053) and non-causal CpG sites (n = 161881) for Aging-GIP1. Two-sided t-test was used. Conservation scores are obtained by Learning Evidence of Conservation from Integrated Functional genomic annotations (LECIF, **b**) and phastCons (**c**). * $P < 0.05$, ** $P < 0.01$, *** $P < 0.001$, **** $P < 0.0001$. **d.** Enrichment of putative causal CpG sites for 12 aging-related traits against transcription-factor-binding sites. Each horizontal bar represents an enriched term. The X-axis shows the -log10(*P*-value), signed by log2 (Odds ratio). The top 10 enriched terms that passed the FDR threshold of 0.05 for each direction are annotated. P values are adjusted for multiple testing using FDR method. **e.** Scatter plot showing the mediation analysis of Aging-GIP1. The total causal effects are shown on X-axis and the direct effects of DNA methylation are shown on Y-axis. The color shows the proportion of DNAm causal effect that is mediated by gene expression. Top CpG-gene pairs are annotated. **f.** Enrichment of the top mediator gene for Aging-GIP1 in GO terms (above dashed line) and KEGG pathways (below the dashed line). The X-axis shows -log(P) for the fisher exact test. One-sided test was used and the P-values are adjusted for multiple testing using FDR method.

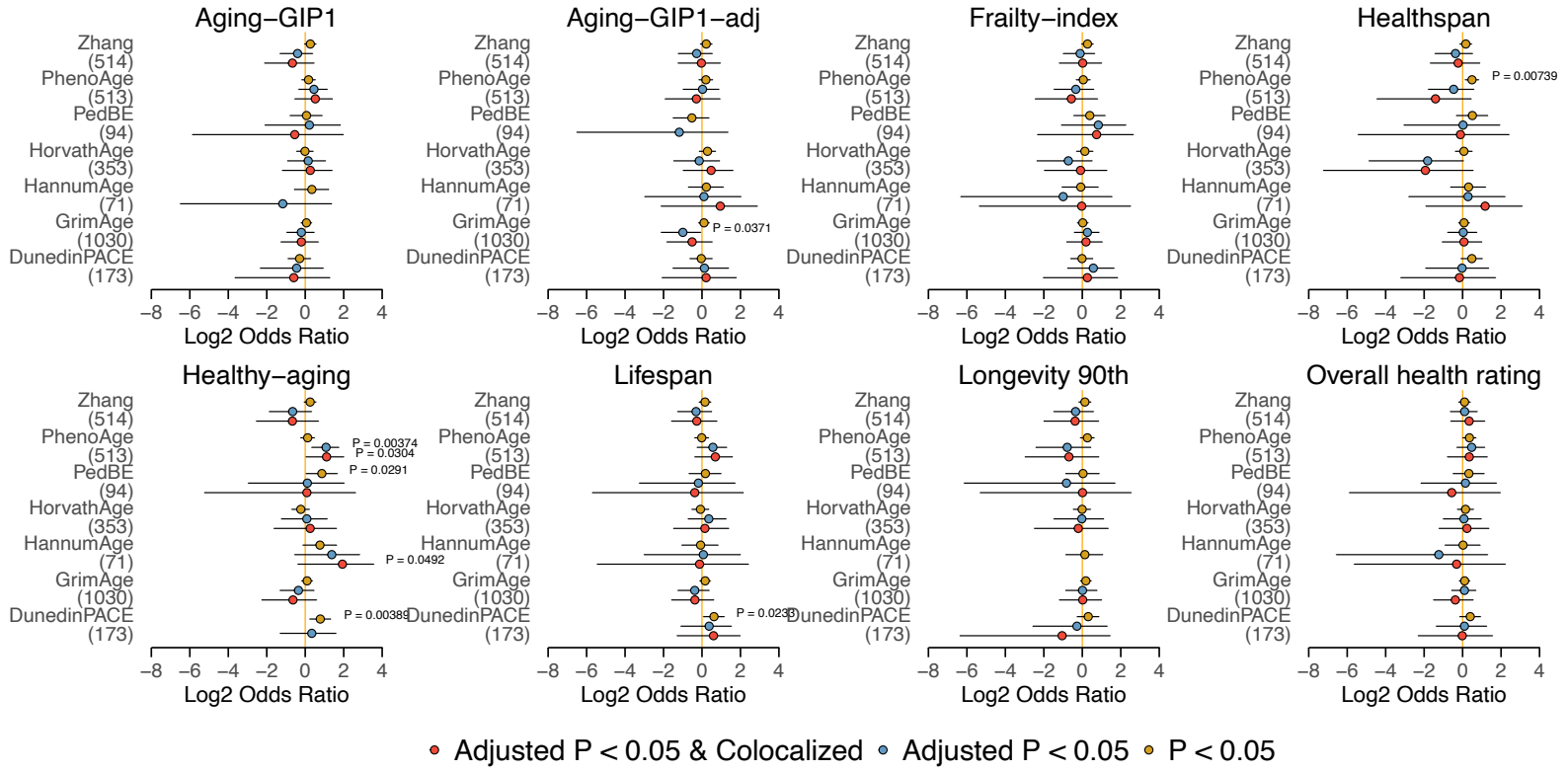
Aging−GIP1
Aging−GIP1−adj
Frailty−index
Healthspan
Healthy−aging
Lifespan
Longevity 90th
Overall health rating
Zhang (514)
PhenoAge (513)
PedBE (94)
HorvathAge (353)
HannumAge (71)
GrimAge (1030)
DunedinPACE (173)
P = 0.0371
P = 0.00739
P = 0.00374
P = 0.0304
P = 0.0291
P = 0.0492
P = 0.00389
P = 0.0239
−8 −6 −4 −2 0 2 4
Log2 Odds Ratio
Adjusted P < 0.05 & Colocalized
Adjusted P < 0.05
P < 0.05

681 **Fig. 3. Existing epigenetic clocks are not enriched with CpG sites causal to aging.** Forest plot
682 shows enrichment of clock sites for six aging clock models in putative causal CpG sites identified
683 by MR for each trait. N of CpG sites for each clock model are annotated in parenthsis under the
684 name of each clock. X-axis shows the log2(Odds Ratio). *P*-values calculated by Fisher's exact test
685 are annotated if $P < 0.05$. The dot shows the estimated value of log2(Odds Ratio). Error bars show
686 95% confidence intervals. Different colors represent the different thresholds for putative causal
687 CpGs. Two-sided Fisher exact test was used. Raw P-values are annotated as none of the results
688 passed the FDR threshold of 0.05.

689

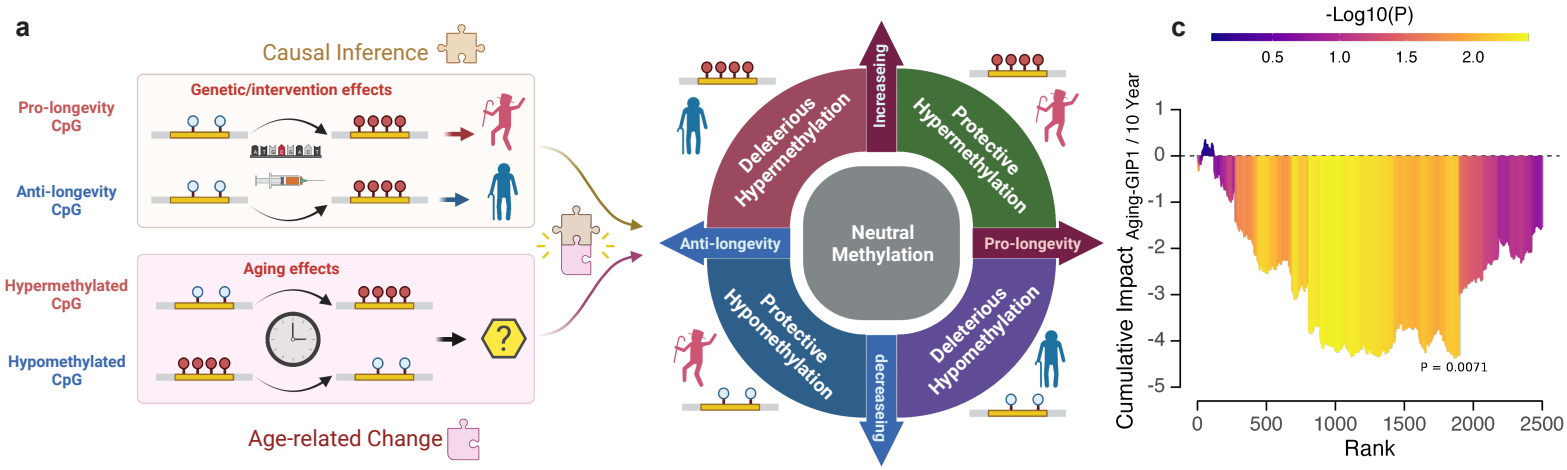
a
Causal Inference
Genetic/intervention effects
Pro-longevity CpG
Anti-longevity CpG
Aging effects
Hypermethylated CpG
Hypomethylated CpG
Age-related Change
Increasing
Deleterious Hypermethylation
Protective Hypermethylation
Anti-longevity
Neutral Methylation
Pro-longevity
Protective Hypomethylation
Deleterious Hypomethylation
decreasing
c
-Log10(P)
0.5
1.0
1.5
2.0
Cumulative Impact Aging-GIP1 / 10 Year
P = 0.0071
Rank

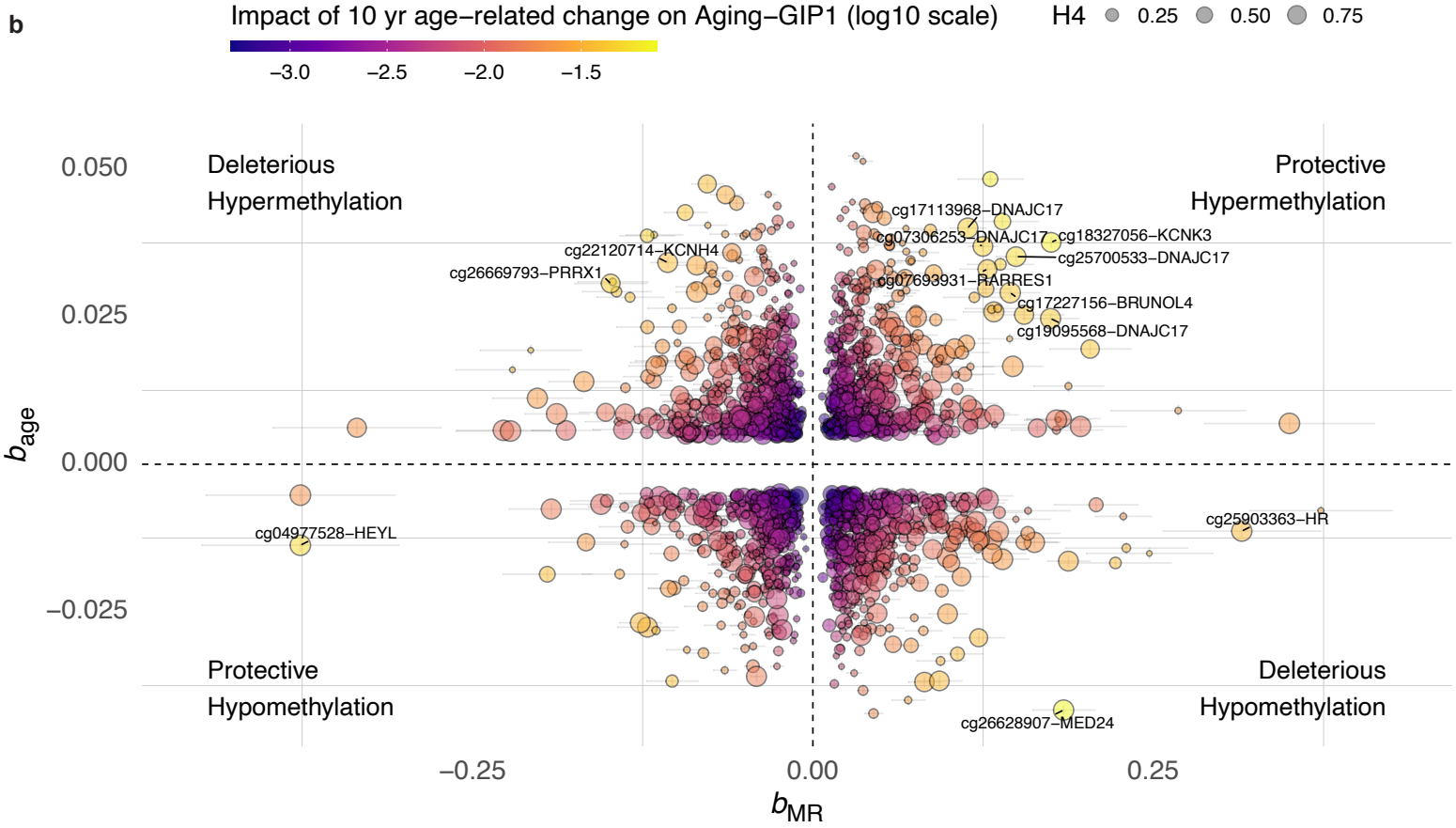
b
Impact of 10 yr age–related change on Aging–GIP1 (log10 scale)
–3.0
–2.5
–2.0
–1.5
H4
0.25
0.50
0.75
Deleterious Hypermethylation
Protective Hypermethylation
Protective Hypomethylation
Deleterious Hypomethylation
cg17113968–DNAJC17
cg07306253–DNAJC17
cg18327056–KCNK3
cg25700533–DNAJC17
cg22120714–KCNH4
cg26669793–PRRX1
cg07693931–RARRES1
cg17227156–BRUNOL4
cg19095568–DNAJC17
cg04977528–HEYL
cg25903363–HR
cg26628907–MED24
0.050
0.025
0.000
–0.025
b_{age}
–0.25
0.00
0.25
b_{MR}

691 **Fig. 4. Integration of causal information and age-associated differential methylation to sep-**
692 **arate protective and damaging epigenetic changes. a.** Schematic diagram showing the method
693 to identify protective and damaging epigenetic changes by integrating MR results and age-related
694 differential methylation. b. Relationship between MR-estimated causal effects (X-axis) and age-
695 related differential methylation (Y-axis) for each significant putative causal CpG identified in Ag-
696 ing-GIP1. The color scheme highlights the expected impact of age-related differential methylation
697 on aging. Error bars show the standard error of *b*. The size reflects the PP-H4. Only CpG sites with
698 adjusted *P*-values < 0.05 and relative PP-H4 > 0.7 are plotted. The CpG sites with the top 10 largest
699 effect sizes are annotated. **c.** Area plots show the total cumulative effect of changes in DNA meth-
700 ylation on Aging-GIP1. X-axis shows the rank of top 3,000 CpG sites based on the magnitude of
701 age-associated differential methylation. Y-axis and the color scheme show the P-value estimated
702 by 10,000 permutation tests. Two-sided Fisher exact test was used.

703

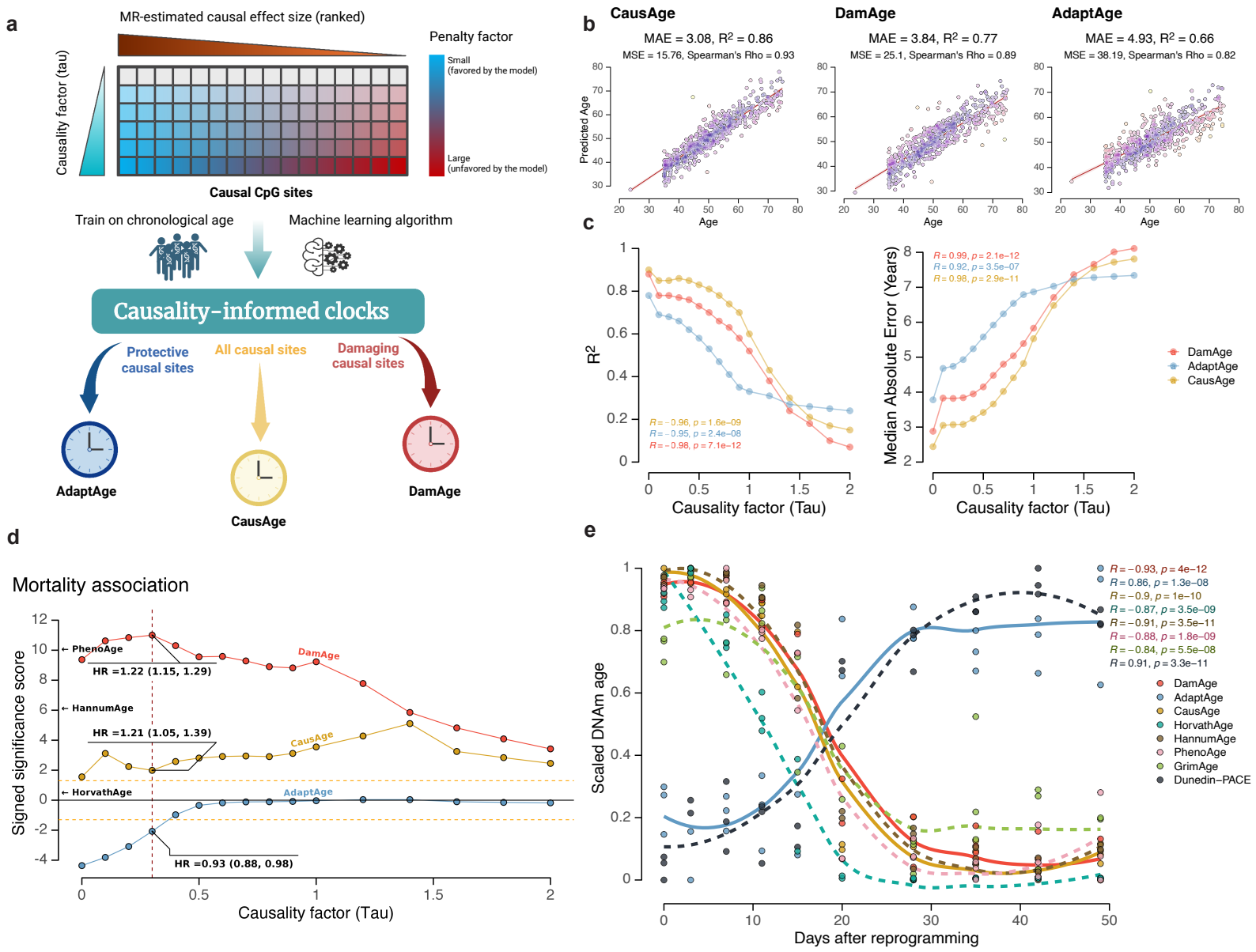
a
MR-estimated causal effect size (ranked)
Penalty factor
Small (favored by the model)
Large (unfavored by the model)
Causality factor (tau)
Causal CpG sites
Train on chronological age
Machine learning algorithm
Causality-informed clocks
Protective causal sites
All causal sites
Damaging causal sites
AdaptAge
CausAge
DamAge
b
CausAge
MAE = 3.08, R2 = 0.86
MSE = 15.76, Spearman's Rho = 0.93
DamAge
MAE = 3.84, R2 = 0.77
MSE = 25.1, Spearman's Rho = 0.89
AdaptAge
MAE = 4.93, R2 = 0.66
MSE = 38.19, Spearman's Rho = 0.82
Predicted Age
Age
c
R2
Causality factor (Tau)
R = −0.96, p = 1.6e−09
R = −0.95, p = 2.4e−08
R = −0.98, p = 7.1e−12
Median Absolute Error (Years)
R = 0.99, p = 2.1e−12
R = 0.92, p = 3.5e−07
R = 0.98, p = 2.9e−11
DamAge
AdaptAge
CausAge
d
Mortality association
Signed significance score
Causality factor (Tau)
PhenoAge
HR =1.22 (1.15, 1.29)
HannumAge
HR =1.21 (1.05, 1.39)
HorvathAge
HR =0.93 (0.88, 0.98)
DamAge
CausAge
AdaptAge
e
Scaled DNAm age
Days after reprogramming
R = −0.93, p = 4e−12
R = 0.86, p = 1.3e−08
R = −0.9, p = 1e−10
R = −0.87, p = 3.5e−09
R = −0.91, p = 3.5e−11
R = −0.88, p = 1.8e−09
R = −0.84, p = 5.5e−08
R = 0.91, p = 3.3e−11
DamAge
AdaptAge
CausAge
HorvathAge
HannumAge
PhenoAge
GrimAge
Dunedin−PACE

Fig. 5. Construction and application of causality-enriched epigenetic clocks. a. Schematic diagram shows the procedure of constructing causality-enriched epigenetic clocks. **b.** Scatter plots show the accuracy of causal clocks on the test set. The X-axis shows the real age of each sample, and the Y-axis shows the predicted age of the same sample based on each clock model. Median absolute error (MAE) and Pearson's R are annotated. **c.** Line plot showing the relationship between causality factor (τ) and clock accuracy measured by MAE and Pearson's R. **d.** Line plot shows the relationship between the causality factor (τ) and -log10(p) for the association with mortality risk (signed by log2(hazard ratio)) estimated from the meta-analysis of FHS and NAS cohorts. Yellow dashed line shows the *P* threshold of 0.05. Hazard ratio of mortality risk for every 10-year increase in age for each clock model and the 95% confidential interval for $\tau = 0.3$ is annotated. Results based on Horvath age, Hannum age, and PhenoAge are also shown by arrows for comparison. **e.** Scatter plots show the application of causal clocks and five other aging clocks to reprogramming of fibroblasts to iPSCs. X-axis shows days after initiating reprogramming. Pearson's R and *P* values are annotated. All P-values reported are raw P-values without multiple testing correction, as the purpose is to compare across different clocks instead of deciding whether the test is significant.

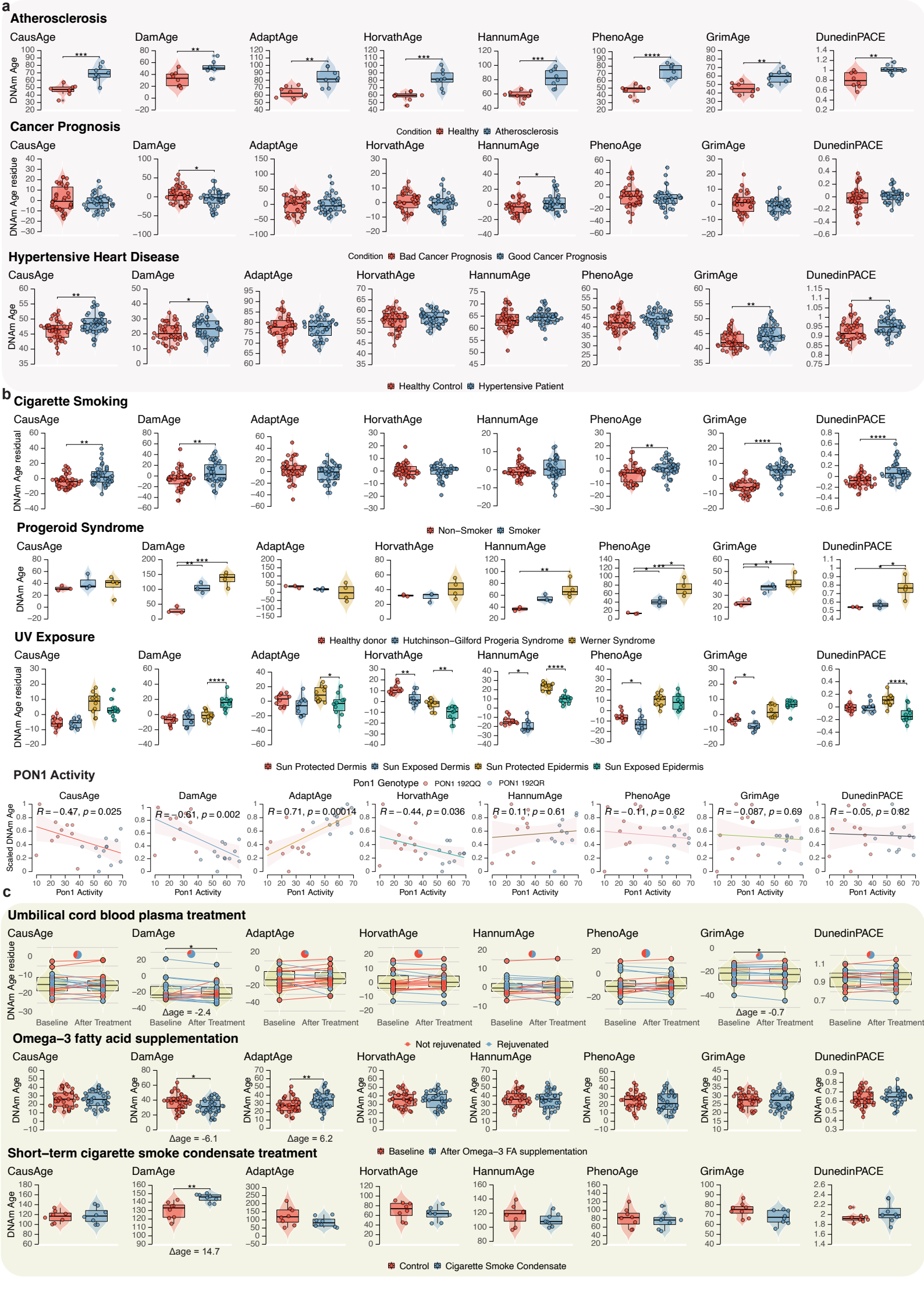
a
Atherosclerosis
CausAge
DamAge
AdaptAge
HorvathAge
HannumAge
PhenoAge
GrimAge
DunedinPACE
DNAm Age
Condition Healthy Atherosclerosis
Cancer Prognosis
DNAm Age residue
Condition Bad Cancer Prognosis Good Cancer Prognosis
Hypertensive Heart Disease
Healthy Control Hypertensive Patient
b
Cigarette Smoking
DNAm Age residue
Non−Smoker Smoker
Progeroid Syndrome
Healthy donor Hutchinson−Gilford Progeria Syndrome Werner Syndrome
UV Exposure
Sun Protected Dermis Sun Exposed Dermis Sun Protected Epidermis Sun Exposed Epidermis
PON1 Activity
Pon1 Genotype PON1 192QQ PON1 192QR
Scaled DNAm Age
R = −0.47, p = 0.025
R = −0.61, p = 0.002
R = 0.71, p = 0.00014
R = −0.44, p = 0.036
R = 0.11, p = 0.61
R = −0.11, p = 0.62
R = −0.087, p = 0.69
R = −0.05, p = 0.82
Pon1 Activity
c
Umbilical cord blood plasma treatment
Baseline After Treatment
Δage = -2.4
Δage = -0.7
Omega−3 fatty acid supplementation
Not rejuvenated Rejuvenated
Δage = -6.1
Δage = 6.2
Short−term cigarette smoke condensate treatment
Baseline After Omega−3 FA supplementation
Δage = 14.7
Control Cigarette Smoke Condensate

Fig. 6. Causality-enriched epigenetic clocks can better capture aging-related effects. a. Box plots show the association between epigenetic age and aging-related conditions, including atherosclerosis (N = 16, significant P values from left to right are 2.79e-4, 0.00619, 0.0011, 2.77e-4, 2.81e-4, 2.75e-5, 0.00231, 0.00413), prostate cancer prognosis (N = 70, significant P values are 0.0394 and 0.044), and hypertensive heart disease (N = 88, significant P values are 0.002, 0.049, 0.002, 0.017). **b.** Box plots show the association between epigenetic age and damaging conditions, including smoking (n = 80, significant P values are 0.004, 0.006, 0.005, 1.01e-14, 7.16e-6), Progeroid Syndromes (n = 10, significant P values are 0.004, 5.55e-4, 0.014, 0.047, 0.002, 0.033, 0.028, 0.006, 0.033, 0.04), and Sun exposure (n = 40, significant P values are 6.1e-4, 7.4e-6, 8.48e-4, 1.18e-5, 7.66e-7, 3.96e-7, 9.78e-5, 0.0256, 2.39e-5, 0.00576, 1.38e-9, 2.82e-6, 4.99e-17, 7.4e-8, 8.91e-5, 1e-8, 1.24e-5, 7.55e-6, 0.0122, 9.47e-4, 1.46e-4). Scatter plots show the correlation between epigenetic age and blood PON1 activity (n = 48). Epigenetic age prediction is rescaled to a 0-1 scale for better comparison. The color scheme shows the PON1 genotype in subjects. Linear regression is performed, and Pearson's R and P values are annotated. **c.** Box plots show the association between epigenetic age and short-term treatments, including the umbilical cord blood plasma treatment (n = 18, significant P values are 0.0481 and 0.0481), 15 months of cigarette smoke condensate (CSC) treatment (n = 16, significant P value is 0.002), and 6-week supplementation of overweight subjects with omega-3 fatty acids (n = 69, significant P value is 0.0087).The effect size of significant effect is annotated. For umbilical cord blood plasma treatment, one-tailed paired sign-test was performed, and the color scheme and the pie chart indicate whether the subject is rejuvenated after treatment based on the corresponding clock. For unpaired box plots, significant pairs based on two-tailed t-test are annotated with stars. * $P < 0.05$, ** $P < 0.01$, *** $P < 0.001$, **** $P < 0.0001$. All reported P values are corrected for multiple testing using FDR method within each clock group. Box plots indicate the median (central line), 25th and 75th percentiles (bounds of box), and the minimum and maximum values (whiskers).

References

1. Gladyshev, V. N. *et al.* Molecular damage in aging. *Nat. Aging* **1**, 1096–1106 (2021).
2. Sziráki, A., Tyshkovskiy, A. & Gladyshev, V. N. Global remodeling of the mouse DNA methylome during aging and in response to calorie restriction. *Aging Cell* **17**, e12738 (2018).
3. Moqri, M. *et al.* PRC2 clock: a universal epigenetic biomarker of aging and rejuvenation. 2022.06.03.494609 Preprint at https://doi.org/10.1101/2022.06.03.494609 (2022).
4. Petkovich, D. A. *et al.* Using DNA Methylation Profiling to Evaluate Biological Age and Longevity Interventions. *Cell Metab.* **25**, 954-960.e6 (2017).
5. Meer, M. V., Podolskiy, D. I., Tyshkovskiy, A. & Gladyshev, V. N. A whole lifespan mouse multi-tissue DNA methylation clock. *eLife* **7**, e40675 (2018).
6. Urban, A. *et al.* Precious1GPT: multimodal transformer-based transfer learning for aging clock development and feature importance analysis for aging and age-related disease target discovery. *Aging* **15**, 4649–4666 (2023).
7. Marioni, R. E. *et al.* The epigenetic clock is correlated with physical and cognitive fitness in the Lothian Birth Cohort 1936. *Int. J. Epidemiol.* **44**, 1388–1396 (2015).
8. Biomarkers of Aging Consortium. Biomarkers of Aging for the Identification and Evaluation of Longevity Interventions. *Cell* (2023).
9. Ying, K. *et al.* Genetic and phenotypic analysis of the causal relationship between aging and COVID-19. *Commun. Med.* **1**, 35 (2021).
10. Kapur, K. Chapter 14 - Principles of Biostatistics. in *Clinical and Translational Science (Second Edition)* (eds. Robertson, D. & Williams, G. H.) 243–260 (Academic Press, 2017). doi:10.1016/B978-0-12-802101-9.00014-4.
11. Davey Smith, G. & Hemani, G. Mendelian randomization: genetic anchors for causal inference in epidemiological studies. *Hum. Mol. Genet.* **23**, R89–R98 (2014).
12. Min, J. L. *et al.* Genomic and phenotypic insights from an atlas of genetic effects on DNA methylation. *Nat. Genet.* **53**, 1311–1321 (2021).

774 13. Richardson, T. G. *et al.* Systematic Mendelian randomization framework elucidates hundreds of CpG
775 sites which may mediate the influence of genetic variants on disease. *Hum. Mol. Genet.* **27**, 3293–
776 3304 (2018).
777 14. Emdin, C. A., Khera, A. V. & Kathiresan, S. Mendelian Randomization. *JAMA* **318**, 1925 (2017).
778 15. Timmers, P. R. *et al.* Genomics of 1 million parent lifespans implicates novel pathways and common
779 diseases and distinguishes survival chances. *eLife* **8**, e39856 (2019).
780 16. Deelen, J. *et al.* A meta-analysis of genome-wide association studies identifies multiple longevity
781 genes. *Nat. Commun.* **10**, 3669 (2019).
782 17. Zenin, A. *et al.* Identification of 12 genetic loci associated with human healthspan. *Commun. Biol.* **2**,
783 41 (2019).
784 18. Atkins, J. L. *et al.* A genome-wide association study of the frailty index highlights brain pathways in
785 ageing. *Aging Cell* **20**, e13459 (2021).
786 19. Timmers, P. R. H. J. *et al.* Mendelian randomization of genetically independent aging phenotypes
787 identifies LPA and VCAM1 as biological targets for human aging. *Nat. Aging* **2**, 19–30 (2022).
788 20. Timmers, P. R. H. J., Wilson, J. F., Joshi, P. K. & Deelen, J. Multivariate genomic scan implicates
789 novel loci and haem metabolism in human ageing. *Nat. Commun.* **11**, 3570 (2020).
790 21. Hemani, G., Tilling, K. & Davey Smith, G. Orienting the causal relationship between imprecisely
791 measured traits using GWAS summary data. *PLOS Genet.* **13**, e1007081 (2017).
792 22. Robinson, J. W. *et al.* An efficient and robust tool for colocalisation: Pair-wise Conditional and Colo-
793 calisation (PWCoCo). 2022.08.08.503158 Preprint at https://doi.org/10.1101/2022.08.08.503158
794 (2022).
795 23. Herzig, S. *et al.* CREB regulates hepatic gluconeogenesis through the coactivator PGC-1. *Nature*
796 **413**, 179–183 (2001).
797 24. Kundaje, A. *et al.* Integrative analysis of 111 reference human epigenomes. *Nature* **518**, 317–330
798 (2015).

799 25. Saldi, T., Cortazar, M. A., Sheridan, R. M. & Bentley, D. L. Coupling of RNA Polymerase II Tran-
800 scription Elongation with Pre-mRNA Splicing. *J. Mol. Biol.* **428**, 2623–2635 (2016).
801 26. Sadler, M. C., Auwerx, C., Lepik, K., Porcu, E. & Kutalik, Z. Quantifying the role of transcript levels
802 in mediating DNA methylation effects on complex traits and diseases. *Nat. Commun.* **13**, 7559
803 (2022).
804 27. Battram, T. *et al.* The EWAS Catalog: a database of epigenome-wide association studies. Preprint at
805 https://doi.org/10.12688/wellcomeopenres.17598.2 (2022).
806 28. Porcu, E. *et al.* Differentially expressed genes reflect disease-induced rather than disease-causing
807 changes in the transcriptome. *Nat. Commun.* **12**, 5647 (2021).
808 29. Ogrodnik, M. & Gladyshev, V. N. The meaning of adaptation in aging: insights from cellular senes-
809 cence, epigenetic clocks and stem cell alterations. *Nat. Aging* **3**, 766–775 (2023).
810 30. McCartney, D. L. *et al.* An epigenome-wide association study of sex-specific chronological ageing.
811 *Genome Med.* **12**, 1 (2020).
812 31. Horvath, S. DNA methylation age of human tissues and cell types. *Genome Biol.* **14**, R115 (2013).
813 32. Ohnuki, M. *et al.* Dynamic regulation of human endogenous retroviruses mediates factor-induced re-
814 programming and differentiation potential. *Proc. Natl. Acad. Sci.* **111**, 12426–12431 (2014).
815 33. Hannum, G. *et al.* Genome-wide Methylation Profiles Reveal Quantitative Views of Human Aging
816 Rates. *Mol. Cell* **49**, 359–367 (2013).
817 34. Levine, M. E. *et al.* An epigenetic biomarker of aging for lifespan and healthspan. *Aging* **10**, 573–591
818 (2018).
819 35. Lu, A. T. *et al.* DNA methylation GrimAge strongly predicts lifespan and healthspan. *Aging* **11**, 303–
820 327 (2019).
821 36. Belsky, D. W. *et al.* DunedinPACE, a DNA methylation biomarker of the pace of aging. *eLife* **11**,
822 e73420 (2022).
823 37. Istas, G. *et al.* Identification of differentially methylated BRCA1 and CRISP2 DNA regions as blood
824 surrogate markers for cardiovascular disease. *Sci. Rep.* **7**, 5120 (2017).

825 38. Toth, R. *et al.* Random forest-based modelling to detect biomarkers for prostate cancer progression.
826 *Clin. Epigenetics* **11**, 148 (2019).
827 39. Bai, C. *et al.* Oviductal Glycoprotein 1 Promotes Hypertension by Inducing Vascular Remodeling
828 Through an Interaction With MYH9. *Circulation* **146**, 1367–1382 (2022).
829 40. Jessen, W. J., Borgerding, M. F. & Prasad, G. L. Global methylation profiles in buccal cells of long-
830 term smokers and moist snuff consumers. *Biomarkers* **23**, 625–639 (2018).
831 41. Heyn, H., Moran, S. & Esteller, M. Aberrant DNA methylation profiles in the premature aging disor-
832 ders Hutchinson-Gilford Progeria and Werner syndrome. *Epigenetics* **8**, 28–33 (2013).
833 42. Vandiver, A. R. *et al.* Age and sun exposure-related widespread genomic blocks of hypomethylation
834 in nonmalignant skin. *Genome Biol.* **16**, 80 (2015).
835 43. López-Otín, C., Blasco, M. A., Partridge, L., Serrano, M. & Kroemer, G. The Hallmarks of Aging.
836 *Cell* **153**, 1194–1217 (2013).
837 44. Lescai, F., Marchegiani, F. & Franceschi, C. PON1 is a longevity gene: Results of a meta-analysis.
838 *Ageing Res. Rev.* **8**, 277–284 (2009).
839 45. Declerck, K. *et al.* Interaction between prenatal pesticide exposure and a common polymorphism in
840 the PON1 gene on DNA methylation in genes associated with cardio-metabolic disease risk—an ex-
841 ploratory study. *Clin. Epigenetics* **9**, 35 (2017).
842 46. Clement, J. *et al.* Umbilical cord plasma concentrate has beneficial effects on DNA methylation
843 GrimAge and human clinical biomarkers. *Aging Cell* **21**, e13696 (2022).
844 47. Tremblay, B. L. *et al.* Epigenetic changes in blood leukocytes following an omega-3 fatty acid sup-
845 plementation. *Clin. Epigenetics* **9**, 43 (2017).
846 48. Estill, M. S. *et al.* Assisted reproductive technology alters deoxyribonucleic acid methylation profiles
847 in bloodspots of newborn infants. *Fertil. Steril.* **106**, 629-639.e10 (2016).
848 49. Bens, S. *et al.* Phenotypic spectrum and extent of DNA methylation defects associated with multi-
849 locus imprinting disturbances. *Epigenomics* **8**, 801–816 (2016).

850 50. Lin, D. *et al.* Characterization of cross-tissue genetic-epigenetic effects and their patterns in schizo-
851 phrenia. *Genome Med.* **10**, 13 (2018).
852 51. Walther, D. M. *et al.* Widespread Proteome Remodeling and Aggregation in Aging C. elegans. *Cell*
853 **161**, 919–932 (2015).
854 52. Burgess, S., Zuber, V., Valdes-Marquez, E., Sun, B. B. & Hopewell, J. C. Mendelian randomization
855 with fine-mapped genetic data: Choosing from large numbers of correlated instrumental variables.
856 *Genet. Epidemiol.* **41**, 714–725 (2017).
857 53. Yavorska, O. O. & Burgess, S. MendelianRandomization: an R package for performing Mendelian
858 randomization analyses using summarized data. *Int. J. Epidemiol.* **46**, 1734–1739 (2017).
859 54. Hemani, G. *et al.* The MR-Base platform supports systematic causal inference across the human phe-
860 nome. *eLife* **7**, e34408 (2018).
861 55. Võsa, U. *et al.* Large-scale cis- and trans-eQTL analyses identify thousands of genetic loci and poly-
862 genic scores that regulate blood gene expression. *Nat. Genet.* **53**, 1300–1310 (2021).
863 56. Zou, H. & Hastie, T. Regularization and Variable Selection Via the Elastic Net. *J. R. Stat. Soc. Ser. B*
864 *Stat. Methodol.* **67**, 301–320 (2005).
865 57. Lehne, B. *et al.* A coherent approach for analysis of the Illumina HumanMethylation450 BeadChip
866 improves data quality and performance in epigenome-wide association studies. *Genome Biol.* **16**, 37
867 (2015).
868 58. Bulik-Sullivan, B. K. *et al.* LD Score regression distinguishes confounding from polygenicity in ge-
869 nome-wide association studies. *Nat Genet* **47**, 291–5 (2015).
870 59. Bowden, J., Davey Smith, G. & Burgess, S. Mendelian randomization with invalid instruments: ef-
871 fect estimation and bias detection through Egger regression. *Int. J. Epidemiol.* **44**, 512–525 (2015).
872 60. Zheng, J. *et al.* Phenome-wide Mendelian randomization mapping the influence of the plasma prote-
873 ome on complex diseases. *Nat. Genet.* **52**, 1122–1131 (2020).
874 61. Bell, B., Rose, C. L. & Damon, A. The Veterans Administration Longitudinal Study of Healthy Ag-
875 ing. *The Gerontologist* **6**, 179–184 (1966).

876 62. Ying, K. *et al.* Biolearn, an open-source library for biomarkers of aging. 2023.12.02.569722 Preprint
877 at https://doi.org/10.1101/2023.12.02.569722 (2023).
878 63. Ying, K. *et al. ClockBase* : a comprehensive platform for biological age profiling in human and
879 mouse. 2023.02.28.530532 Preprint at https://doi.org/10.1101/2023.02.28.530532 (2023).

880